





Original Article



Using satellite-derived land surface temperatures to clarify the spatiotemporal warming trends of the Alborz Mountains in northern Iran

ROSHAN Gholamreza¹  <https://orcid.org/0000-0003-4097-6940>; e-mail: ghr.roshan@gu.ac.ir

SARLI Reza²  <https://orcid.org/0000-0001-5027-6513>; e-mail: reza.sarli.sd@student.urk.edu.pl

GHANGHERMEH Abdolazim¹  <https://orcid.org/0000-0002-5866-4972>; e-mail: a.ghangherme@gu.ac.ir

TAHERIZADEH Mehrnoosh³  <https://orcid.org/0000-0001-9204-8471>; e-mail: Mehrnooshtahereezadeh@gmail.com

NIKNAM Arman^{3*}  <https://orcid.org/0000-0001-8830-4794>;  e-mail: Niknam.Arman@stud.u-szeged.hu

*Corresponding author

¹ Department of Geography, Golestan University, Gorgan 49138-15759, Iran

² Department of Forest Resources Management, Faculty of Forestry, University of Agriculture in Krakow, AL. 29 Listopada 46,31-425 Kraków, Poland

³ Department of Geoinformatics, Physical and Environmental Geography, University of Szeged, Szeged 6722, Hungary

Citation: Roshan G, Sarli R, Ghanghermeh A, et al. (2024) Using satellite-derived land surface temperatures to clarify the spatiotemporal warming trends of the Alborz Mountains in northern Iran. *Journal of Mountain Science* 21(2). <https://doi.org/10.1007/s11629-023-8384-z>

© The Author(s) 2024.

Abstract: The Alborz Mountains are some of the highest in Iran, and they play an important role in controlling the climate of the country's northern regions. The land surface temperature (LST) is an important variable that affects the ecosystem of this area. This study investigated the spatiotemporal changes and trends of the nighttime LST in the western region of the Central Alborz Mountains at elevations of 1500–4000 m above sea level. MODIS data were extracted for the period of 2000–2021, and the Mann–Kendall nonparametric test was applied to evaluating the changes in the LST. The results indicated a significant increasing trend for the monthly average LST in May–August along the southern aspect. Both the northern and southern aspects showed decreasing trends for the monthly average LST in October, November, and March and an increasing trend in other months. At all elevations, the average decadal change in the monthly average LST was more severe along the southern aspect (0.60°C) than along the northern

aspect (0.37°C). The LST difference between the northern and southern aspects decreased in the cold months but increased in the hot months. At the same elevation, the difference in the lapse rate between the northern and southern aspects was greater in the hot months than in the cold months. With increasing elevation, the lapse rate between the northern and southern aspects disappeared. Climate change was concluded to greatly decrease the difference in LST at different elevations for April–July.

Keywords: Global warming; Mountainous areas; Lapse rate; Surface air temperatures; Alborz

1 Introduction

Mountains are among the most influential geographic features for the formation of climatic patterns and are highly sensitive to climate change (Rousta et al. 2022; Steiger et al. 2022). Many studies

Received: 03-Oct-2023

Revised: 27-Dec-2023

Accepted: 09-Jan-2024

have shown that climate change has had many environmental consequences in mountainous and high-elevation areas, such as reduced biodiversity (Nabizada et al. 2022; Rousta et al. 2021; Lau et al. 2010), shrinking habitats (Freeman et al. 2018; Parmesan 2006), and the retreat of glaciers (Huss and Hock 2018; Huss et al. 2017; Kuhn 1989; Marzeion et al. 2018; Scherrer et al. 2012; Duan et al. 2019; Yousefizadeh et al. 2022). Mountains are considered a main source of freshwater storage (Vaghefi et al. 2019; Barnett et al. 2005; Gupta et al. 2020), which is often distributed in the form of snow and ice. However, climate change has reduced the ice mass in mountainous regions, which can eliminate water resources for downstream regions where billions of people live (Bradley et al. 2006; Viviroli et al. 2011). One of the consequences of climate change is an earlier start to warm seasons, which accelerates the melting of snow and ice (Musselman et al. 2017; Sabziparvar et al. 2019), especially in areas where the annual temperature is close to the melting threshold. The smallest change in ambient temperature can have a large feedback effect on the hydrologic cycle in such regions (Haerberli and Weingartner 2020). Various studies have shown that the elevation has a major effect on the heating rate of mountainous areas (Diaz and Bradley 1997; Pepin et al. 2015; Wang et al. 2018; Rangwala and Miller 2012; Viviroli et al. 2020). Mountainous areas do not always heat up faster than lowland areas, but a systematic process is behind the variability. The temperature increases faster at the snowline than in the surrounding areas due to the snow–albedo interaction (Pepin and Seidel 2005; Sambuco et al. 2020). The change in heating rate with elevation can affect the static stability of the atmosphere (Frierson 2006), which alters precipitation patterns and can affect human activities (Mansourmoghaddam et al. 2023; Mansourmoghaddam and Rousta 2023). Thus, any systematic change in the effect of elevation is of great importance to understanding the changes in temperature in mountainous areas (Nabizada et al. 2023; Olafsson and Rousta 2021). There is no official definition of elevation-dependent warming (EDW), but Rangwala et al. and Miller (2012) and Pepin et al. (2015) have defined it as any change in the temperature rate that is systematically observed with increasing height. Although not always the case, the temperature rate often increases in high-elevation areas. EDW is a very complex process (Rangwala and

Miller 2012) affected by many mechanisms, including water vapor modulation of downward thermal radiation (Rangwala et al. 2013), cloud patterns and cover (Xiao et al. 2020) aerosol loading (Lau et al. 2010) and snow–ice albedo feedback (Minder et al. 2010).

Iran is a country with various topographies and geographic features such as plains, mountains, deserts, and forests, each of which affects climatic patterns from the local to the regional scale (Rousta et al. 2017). The Alborz Mountains have influenced the formation of a humid to very humid climate along their northern aspect and a dry to semiarid climate along their southern aspect. They have been included in many previous studies examining the effects of climate change in Iranian mountains (Azizi et al. 2013; Ghehsareh Ardestani and Heidari Ghahfarrokhi 2021; Arsalani et al. 2022; Janizadeh et al. 2023; Naseri et al. 2021). Given that most lowland areas surrounding mountains in Iran are semiarid to arid, any climate change–related effects that may reduce mountain water resources have critical implications for the country’s agriculture and society (Emadodin et al. 2019; Asakereh and Ashrafi 2023). To ensure appropriate planning and preparation for climate-related water scarcity in the future, a downscaled approach to understanding regional-scale changes in temperature and hydrology is critical. About 16% of Iran’s population, primarily those living in the provinces of Alborz and Tehran, directly depend on water resources originating from the Central Alborz Mountains, and water scarcity has become an acute concern in this area (Mansouri Daneshvar et al. 2019; Abe 2013; Tang et al. 2022).

This study aimed to use satellite data to establish spatiotemporal patterns of changes in surface temperature over the last two decades, in an effort to extrapolate the effects of climate change on the future water security of this region. One innovative approach involves harnessing data from the Moderate Resolution Imaging Spectroradiometer (MODIS) satellite sensor, coupled with the application of the Mann-Kendall nonparametric test.

One crucial factor in the interactions between the surface and atmosphere is land surface temperature (LST), which plays a significant role in global change and heat balance studies and might simulate climate change (Tan et al. 2019). Space-based sensors provide high-resolution surface images of earth for environmental investigations (Taherizadeh et al. 2023). LST monitoring using thermal infrared remote sensing data accelerates the development of LST

estimation methods. Since 2000 and 2002, the MODIS on the Terra or Aqua satellites has provided long-term LST output with high data accuracy and temporal frequency (Li et al. 2013). Validation tests have shown that MODIS LST estimation has a high level of accuracy, with an absolute error ranging from 1.0 K to 3.0 K (Duan et al. 2019). Therefore, the Intergovernmental Panel on Climate Change (IPCC) advises integrating long-term LST data from satellite remote sensing in global warming research because of its importance. This integration might assist in overcoming deficiencies in weather station air temperature records (Aguilar-Lome et al. 2019).

The MODIS LST data are commonly employed for the estimation of air temperature (Yang et al. 2017; Zhang et al. 2016). Several studies have been conducted on a regional scale. For instance, studies in the Alps (Colombi et al. 2007), the central Himalayas (Li et al. 2013), the Ganga River Basin (Mal et al. 2022), and high-mountain Asia (Rani and Mal 2022) indicate a rising trend in LST. Over the past 20 years, LST has increased more in the highlands than in the lowlands. The aforementioned investigations have validated the performance of MODIS sensor daytime and nighttime LST data for the Terra and Aqua satellites.

Several research papers in Iran have used satellite observations to examine Land Surface Temperature (LST) in different areas (Didari et al. 2017). In a mountainous region such as Iran, the utilization of satellite products is crucial since only 6% of its ground stations are situated at an elevation of over 2000 m. However, a review of the literature shows that fewer researchers have investigated LST of Iran at night using satellite products or station data (Sarhan et al. 2023). In recent years, the horizontal resolution of LST has also improved significantly and is now available for a longer time.

In the following, the Mann–Kendall nonparametric test was applied to evaluate changes in LST. Trend analysis is a vital method for assessing time-series data. Mann initially introduced the Mann–Kendall nonparametric test in 1945, and Kendall subsequently improved it in 1975. This test utilizes data ranking to analyze trends in hydrological and meteorological datasets (Hussain et al. 2019). Kumar et al. (2005) in Italy, Tayanç et al. (2009) in Turkey, Seleshi and Zanke (2004) in Ethiopia, Domonkos and Tar (2003) in Hungary, and Domroes and El-Tantawi (2005) in Egypt have all demonstrated patterns in the time series of minimum and maximum temperatures. The innovation of the current study lies in the

combination of remote sensing technology (MODIS data) and statistical analysis (Mann–Kendall test) to assess and quantify changes in land surface temperature over the years.

The research focuses on comparing changes in LST at similar altitude levels between the northern and southern aspects of the Middle Alborz. Previous studies on Alborz did not examine alterations in LST at comparable altitudes or based on station air temperature. Instead, they relied on scattered stations at different altitudes. This made it difficult to compare LST changes at similar levels across the two aspects. Secondly, it is important to note that a new and unique concept is being examined in the area, which involves examining changes in lapse rate trends and comparing them between the northern and southern aspects. While previous studies have assessed temperature change trends in this region, they have not yet noticed the impact of global warming on the trend of lapse rates. As known, changes in LST patterns can be influenced by both local and extra-local parameters. Among these local parameters is the moisture and hydrological regime of the region. While various moisture indicators have been utilized for this area, the Topographic Wetness Index (TWI) stands out as an indicator that allows the evaluation of the region's moisture regime based on topographical position. Although previous Alborz studies have applied TWI for topics like flood and erosion zoning (Vakili Tajareh et al. 2022) or soil organic carbon content (Maleki et al. 2014), identifying the LST variability pattern according to the moisture regime (derived from TWI at different height scales) is a relatively unexplored area not found in prior Alborz research.

2 Materials and Methods

2.1 Study area

The Central Alborz Mountains are the highest mountain range in Iran and are located to the north of Iran (35°50′–36°40′ N, 50°50′–52°50′ E). They have a steep elevation gradient with a lowest point of 26 m above sea level (ASL) near the Caspian Sea and a highest point of 5671 m ASL at the peak of Mount Damavand. The northern (N) aspect receives large amounts of precipitation at 500–1500 mm/yr. The vegetation cover mostly comprises Hyrcanian forests up to ~2400 m ASL but in some cases may reach 2850

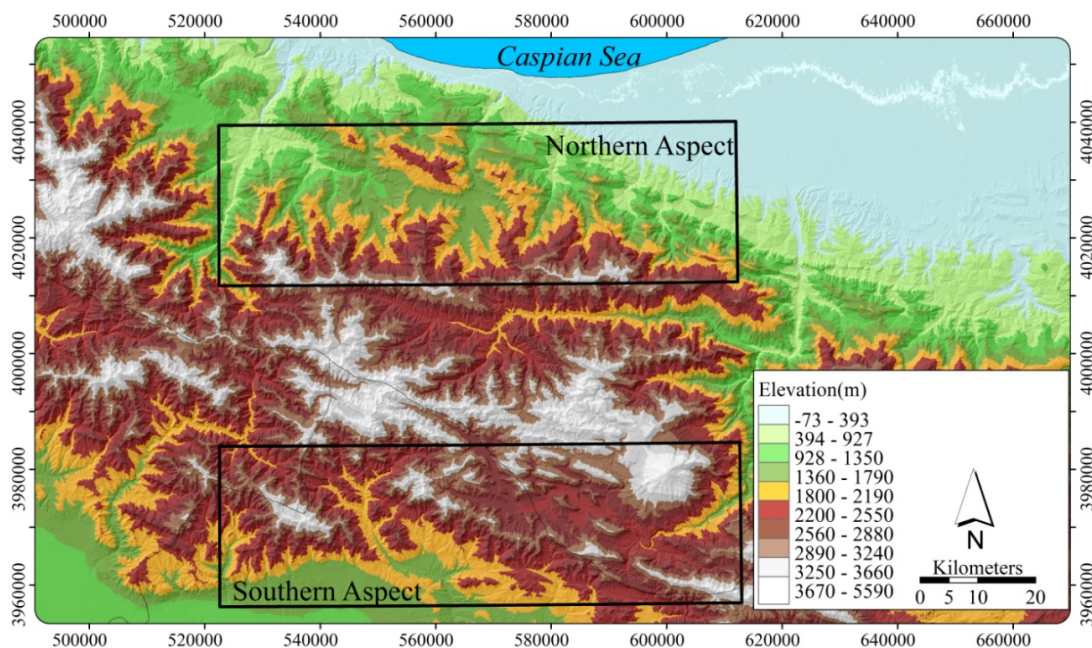


Fig. 1 Geographic location and topography of the study area.

m ASL (Zemp et al. 2019). Vascular plants reach up to ~4850 m ASL on Mount Damavand (Noroozi and Körner 2018). The climate is humid warm temperate. In contrast, the climate on the southern (S) aspect is continental semiarid, where summer droughts are prominent. Here, the precipitation ranges from 25 to 2000 mm/yr. At high elevations, the climate and precipitation are Mediterranean with considerable amounts of snowfall during the late autumn, winter and early spring. Thus, the precipitation patterns across the Alborz Mountains are strongly influenced by the topography, which creates an orographic uplift to the north and a rain shadow to the south (Zemp et al. 2019). The Takhte–Soleiman Glacier, which is the largest in Iran (7.55 km²), is in the Central Alborz Mountains (Sabziparvar et al. 2019; Zemp et al. 2019). This mountain range is an exceptionally important source of water for the surrounding drier regions and large urban centers such as Tehran. The western region of the Central Alborz Mountains (36.12° N, 51.75° E) was selected as the study area (Fig. 1), which was further divided into N and S aspects.

2.2 Extraction of the LST from satellite data

The Moderate Resolution Imaging Spectrometer (MODIS) is a sensor that captures images of the entire Earth once every 2 days aboard the Terra satellite, which orbits Earth every 99 min. MODIS uses all 36 bands for daytime imaging and bands 20–36 (i.e.,

thermal bands) for nighttime imaging. The Terra satellite normally passes over Iran in the morning at 10:30–11:30 am local time (LT) and in the evening at about 22:30 pm LT. In this study, MODIS observational data over Iran at 22:30 pm LT were used to extract monthly-scale land surface temperature (LST) characteristics for the period of 2001–2021. Six elevation levels common to the N and S aspects were identified covering the ranges of 1000–4000 m ASL. The changes in LST were determined according to elevation across the various landscape components. Table 1 presents further details on the areal coverage (hectares) and mean slope gradients (degrees) of the elevation levels in the study area.

Table 1 Area (hectares) and mean slope gradient (degrees) for elevation levels on the northern and southern aspects of the study area

Elevation (m a.s.l.)	N	S
1000-1500	46357.2	9522.0
1500-2000	65248.2	40196.9
2000-2500	41604.9	68367.7
2500-3000	24896.1	85805.7
3000-3500	10986.0	36339.1
3500-4000	1124.5	7484.8
Average (hectares)	31702.82	41286.03
Slope gradient (degrees)	21.7	22.7

Google Earth Engine was used to download MODIS image data from the Terra satellite with the code MOD11A2. The LSTs were extracted from thermal infrared data in bands 31 (10.78–11.28 μm) and 32 (11.77–12.27 μm). The MOD11A2 product provides

LST/emissivity 8-Day L3 Global 1 km data, which include the LST at a spatial resolution of 1 km, scale of 0.02, 16-bit unsigned integer, and 8-day time combination. The data were combined with 240 images for each landscape site to calculate the monthly average LSTs. The LST data were processed by using Visual Basic for Applications programming in Excel, and statistical analysis was then performed. In this study, only the nighttime LST data were used.

Furthermore, soil temperature data was collected from four stations in the study area at a depth of 5 cm. This data was used to validate the extracted LST values. The validation process employed various statistical metrics such as Mean Squared Error (MSE), Root Mean Square Error (RMSE), R-squared (R^2), Adjusted R-squared, Mean Absolute Percentage Error (MAPE), and Durbin-Watson (DW). The calculation details for these statistical methods are outlined in various sources, and you can find direct references to these sources in (Ewane and Lee 2017; Ghanghermeh et al. 2019; Bonshoms et al. 2022; Li et al. 2023).

2.3 Topographic Wetness Index (TWI)

The main focus of this research is to examine the changes in spatio-temporal patterns of LST within the study area. Several factors can influence the changes in LST patterns in this region. The role of land use and its evolving process is evident in governing the spatio-temporal changes in LST. Additionally, moisture and hydrological patterns may also impact LST changes. Therefore, the objective of this study is to illustrate the significant differences in moisture regimes experienced with changes in altitude levels in the two studied slopes. To uncover the alterations in the moisture regime at different levels within the two slopes, the Topographic Wetness Index (TWI) was employed, and the calculation details of this index are provided in this section of the research. Furthermore, the subsequent part of the study will outline the procedures for determining land use and subsequently present the results of assessing these changes over time.

But the TWI is a terrain-based hydrological model used in geography and environmental science to assess the wetness of a landscape. It proves particularly valuable in hydrological modelling, watershed analysis, and land-use planning, allowing for the quantification of topographic controls on hydrological processes (Beven and Kirkby 1979; Sørensen et al. 2006). The TWI has the potential to influence climatic variables,

such as temperature and humidity. Areas with high TWI typically experience lower temperatures and higher moisture levels due to the movement of water towards these regions, resulting in cooling effects on the terrain and an elevation in surrounding humidity (Chaplot et al. 2000). In this context, the TWI has been calculated using a gridded Digital Elevation Model (DEM) layer (cell size = 12.5 square meters) for a specific geographic location, based on slope, flow direction, flow accumulation, and the tangent of the slope. Regions with lower TWI values correspond to areas with lower moisture content, while those with higher TWI values indicate higher moisture content. For specific details on the calculations, please refer to the following equations in Fig. 2. Fig. 2 shows the flow chart of the calculation steps of the TWI.

In this workflow, we have started by projecting the Digital Elevation Model (DEM) to establish its spatial relationship. Then, we applied a DEM filling process to address any depressions or sinks in the terrain. The flow direction was determined, and we computed the flow accumulation to determine the number of contributing cells at each location. We calculated slope values in degrees and converted them to radians. To account for slope values, we introduced a conditional statement. We employed the tangent of the slope if it was greater than zero. Otherwise, we substituted a small value (0.001) to prevent undefined pixels. The flow accumulation was calculated and scaled. Border pixels with zero flow accumulation were adjusted by adding 1. After scaling, the natural logarithm of the difference between the scaled flow accumulation and the slope's tangent served as the basis for calculating the Topographic Wetness Index (TWI). Proper consideration was given to potential zero slope values.

2.4 Production of urban land use map

The study utilized very high-resolution satellite imagery from Google Earth (GE) for sample extraction and creating a reference dataset. The reference dataset, serving as training and validation data, was generated through visual inspection of GE imagery for the year 2021, with a forward revision process applied to earlier years (2001 to 2020). To produce multi-temporal land use maps, Landsat satellite time series and spectral-temporal metrics (STMs) were employed. The Google Earth Engine (GEE) platform facilitated tasks such as image collection, preprocessing, feature extraction, classification, and accuracy assessments. Landsat

surface reflectance products with minimal cloud cover between March 1 and October 30 were selected. Various STMs, including percentile metrics, standard deviation, mean, and minimum/maximum of spectral bands, were calculated. For land use classification, training samples, STMs, and the random forest (RF) algorithm were utilized (Heidarlou et al. 2023). RF, a tree-based machine learning algorithm, was chosen for its effectiveness in remote sensing datasets. A total of 1143 samples representing six land use and land cover (LULC) classes were collected: Forests, Shrublands, Grasslands, Croplands, Non-Vegetated Lands, and Urban and Built-up Lands. The samples in the reference dataset were randomly divided into training (70%) and testing (30%) subsets.

The training samples (Table 2) and STMs (Table 3) were used to train a random forest (RF) model for LULC

classification. An RF model is a machine learning model based on decision trees; RF models perform excellently in similar studies due to their capability to distinguish and map classes with similar spectral attributes (Chang et al. 2020; Nasiri et al. 2023).

The accuracy assessment of land use maps is essential following satellite image classification and holds significance for various users. Aerial photographs, existing thematic maps, or field operations can be utilized to generate a real-world map. The most common method for analysis involves using an error matrix, comparing two sets of data: one group consists of classes resulting from classification, and the other comprises ground-truth or reference data. This square-shaped matrix allows for the examination of two types of errors: omission errors, indicating pixels that should have been classified into hypothetical class

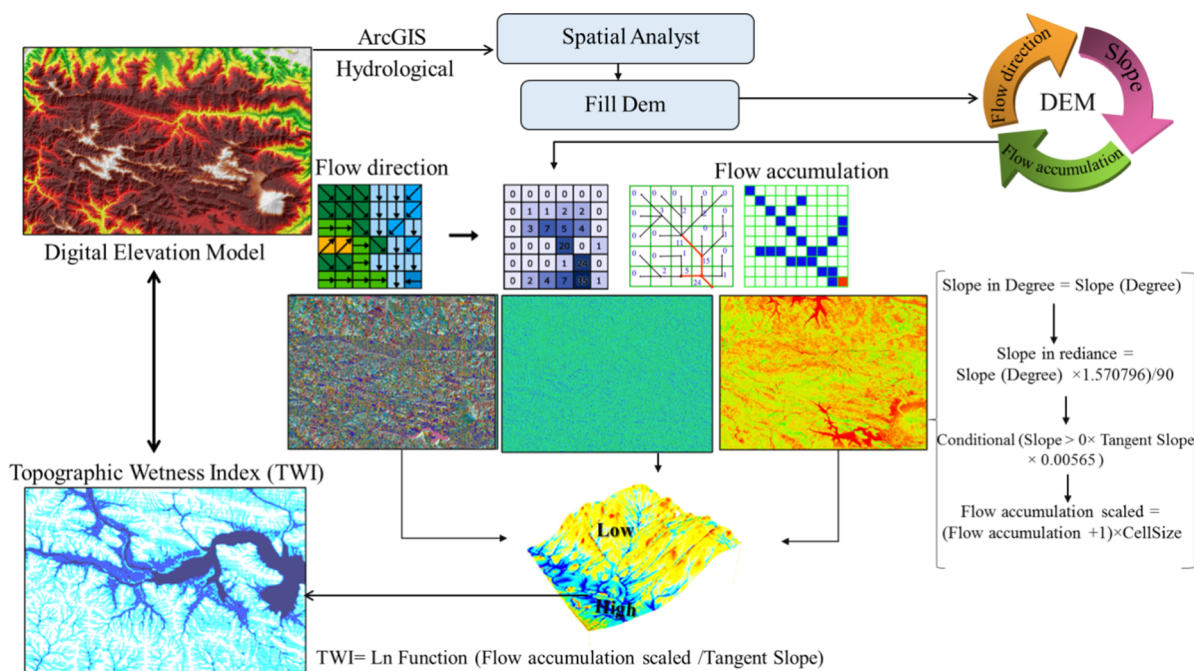


Fig. 2 Steps to calculate the topographic wetness index.

Table 2 Introducing the 2021 base reference dataset with a 30 m pixel size, for sample preparation across different time points

LULC	Training samples		Validation Samples	
	Number of Samples	Number of Pixels	Number of Samples	Number of Pixels
Forest	174	1406	86	614
Grasslands	118	902	62	398
Cropland	118	902	62	398
Non-Vegetated Lands	83	587	47	263
Shrublands	104	776	56	344
Urban and Built-up Lands	83	587	47	263

Table 3 Landsat data at different time points.

Sensor	Time	Bands	Spatial resolution	Wavelength (µm)	Radiometric resolution
TM (Landsat 5)	2001 to 2012	7	30 m	0/4 to 1/4	16 Bit
OLI (Landsat 8)	2013 to 2021	11			

1 but were placed in another class, and commission errors, representing pixels that are not actually part of class 1 but were erroneously classified as such. The diagonal elements of the matrix correspond to pixels correctly classified, while other elements highlight the two types of errors (Lu et al. 2004).

One significant application of the error matrix is the calculation of overall map accuracy. The estimation of accuracy is crucial for understanding the obtained results and making informed decisions. The most commonly used accuracy estimation parameters include overall accuracy, producer’s accuracy, user’s accuracy, and the Kappa coefficient. From a probability theory perspective, overall accuracy may not be a robust criterion for evaluating classification results due to the significant influence of chance. Therefore, the Kappa coefficient is often preferred, as it considers misclassified pixels and provides a more reliable assessment (Pflugmacher et al. 2019).

In the stage of determining map accuracy, it becomes clear to what extent the classified map aligns with the ground truth. The value and utility of each produced map depend on its accuracy (Baumann et al. 2015). The widely used and standard method for determining the accuracy of classified maps involves using the error matrix. For the accuracy assessment of these maps, ground truth information or training areas is required. Testing areas typically include randomly selected samples of relevant land cover types, following statistical criteria to ensure sufficient samples for estimating accuracy and class variances. In the error matrix, reference data (columns of the matrix) are compared with classified data (rows of the matrix).

Another method is using overall accuracy, a metric employed to express the accuracy of results obtained from various classification methods. In research and projects where the comparison of classification accuracy is crucial, the Kappa coefficient is often preferred due to its emphasis on misclassified pixels. The Kappa index is calculated using specific formulas. Additionally, overall accuracy, producer’s accuracy, user’s accuracy, and the F1 score are commonly used parameters for accuracy estimation. It is acknowledged that overall accuracy may not be an ideal measure due to the significant role of chance. Thus, the Kappa coefficient is often preferred in research and projects where comparing the accuracy of different classification methods is essential.

Accuracy assessments were conducted using validation samples and confusion matrices, with

metrics such as overall accuracy (OA), kappa coefficient, producer’s accuracy (PA), user’s accuracy (UA), F-score, and commission/omission errors calculated. The F-score is a per-class metric representing the harmonic mean of user and producer’s accuracies, while OA and the kappa coefficient measure the overall agreement between classified and reference data. OA can be calculated using Eq. (1):

$$OA = 1/N \times \sum Pii \tag{1}$$

In most cases, the Kappa index is used to assess the accuracy of results obtained from various classification methods. Due to the shortcomings affecting overall accuracy, the Kappa index is often utilized in research projects and executive tasks where the comparison of the accuracy of different classifications is of interest. This is because the Kappa index takes misclassified pixels into account (Petropoulos et al. 2011). The Kappa index is calculated using Eq. (2):

$$K = P_o - P_e / 1 - P_e \tag{2}$$

Where: P_o = Probability of agreement. P_e = Probability of random agreement.

$$\emptyset 1 = \frac{1}{N} \sum_{i=1}^m Pii \tag{3}$$

$$\emptyset 2 = \frac{1}{N^2} \sum_{i=1}^m pii \cdot pi \tag{4}$$

Where: Pii = Main diagonal element corresponding to class i . m = Number of classes. N = Total number of test samples across all classes. pi = Sum of elements in the i -th column, representing the total number of instances predicted as class i .

2.5 Mann–Kendall nonparametric test

The Mann-Kendall test is widely used to quantify the significance of trends in meteorological time series (Gocic and Trajkovic 2013; Roshan et al. 2016; Frimpong et al. 2022; Nigrelli and Chiarle 2023). The Mann–Kendall nonparametric test was used to identify significant trends in the LST. The parameter S represents the difference between each observation and all observations afterward (Jaiswal et al. 2015; Gadedjisso-tossou and Adjegan 2021; Monforte and Ragusa 2022):

$$S = \sum_{k=1}^{n-1} \sum_{j=k+1}^n \text{sgn}(x_j - x_k) \tag{5}$$

where n is the number of observations of the series and x_j and x_k are the j th and k th data, respectively, of the series. The sgn function is given by

$$\text{sgn}(x_j - x_k) = \begin{cases} +1 & \text{for } (x_j - x_k) > 0 \\ 0 & \text{for } (x_j - x_k) = 0 \\ -1 & \text{for } (x_j - x_k) < 0 \end{cases} \quad (6)$$

The variance of S is calculated by using one of the following relations according to n :

$$\text{Var}(S) = \frac{n(n-1)(2n+5) - \sum_{i=1}^l t(t-1)(2t+5)}{18} \quad \text{for } n > 10 \quad (7)$$

$$\text{Var}(S) = \frac{n(n-1)(2n+5) - (n2+5)}{18} \quad \text{for } n < 10 \quad (8)$$

where l is the number of sequences containing at least one duplicate data and t is the frequency of data with the same value in a sequence. Finally, the Z statistic is extracted by using one of the following equations according to the value of S :

$$Z = \frac{S-1}{\sqrt{\text{Var}(S)}} \quad \text{for } S > 0 \quad (9)$$

$$Z = 0 \quad \text{for } S = 0$$

$$Z = \frac{S+1}{\sqrt{\text{Var}(S)}} \quad \text{for } S < 0 \quad (10)$$

Assuming two domains of the trend test, the null hypothesis is accepted if the following condition is met:

$$|Z| < Z_{\frac{\alpha}{2}} \quad (11)$$

where α is the significance level that is considered for the test and Z_{α} is the standard normal distribution statistic at the significance level of α , which becomes $\frac{\alpha}{2}$ because of the two domains of the test.

3 Results

3.1 Spatiotemporal variability of LSTs across the study area

3.1.1 Validation of LST data based on soil temperature observation data

In this part of the study, we evaluated the accuracy of LST data by comparing it with soil temperature data at a depth of 5 cm. It should be noted that LST indicates the temperature of the Earth's surface, so it's more appropriate to validate it with soil temperature data instead of air temperature data. We used soil temperature data from four meteorological stations located in the study area. Table 4 displays the results, which demonstrate the validity and precision of LST data. According to the R^2 and Adjusted r values, the lowest output,

at 0.946, belongs to the Baladeh station, while the highest, at 0.972, is for Kojur. Regarding error, Kojur exhibits the lowest MSE (1.276) and RMSE (1.130), and the joint lowest MAPE (44.598) is observed for Alasht and Siahbisheh. The Durbin-Watson (DW) values, which range between 0 and 4, indicate no serial correlation between residuals, with all stations falling within the acceptable range of 1.5 to 2.5 (Table 4). Fig. 3 illustrates the distribution of LST data relative to soil temperature (ST) values along with their linear regression equation.

3.1.2 Monthly and annual trends

The spatiotemporal variability of the monthly and annual average LSTs was analyzed for different elevation levels of the study area. Over all elevation levels, the annual average LST was lower on the N aspect (2.03°C) than on the S aspect (2.41°C). However, the lowest monthly average LST (-17.41°C) was observed on the S aspect in January at an elevation level of 4000 m, and the highest monthly average LST (25.43°C) was observed on the S aspect in July at an elevation level of 1500 m (Fig. 4a). The minimum monthly average LSTs of both the N and S aspects were observed in January at -8.87°C and -10.45°C, respectively. The maximum monthly average LSTs of the N and S aspects were observed in July at 12.30°C and 15.37°C, respectively (Fig. 4c). During the warm seasons (i.e., spring and summer), the monthly average LST was lower on the N aspect than on the S aspect; in contrast, during the cold seasons (i.e., autumn and winter), the monthly average LST was lower on the S aspect than on the N aspect. At lower elevation levels (1500 and 2000 m), the annual average LST was lower on the N aspect; at higher elevation levels (>2000 m), the annual average LST was lower on the S aspect (Fig. 4b).

An important topic in climate change studies is analyzing the variability of climatic components.

Table 4 Validation of LST data based on soil temperature observation data for 4 selected stations

Stations	Alasht	Baladeh	Kojur	Siahbisheh
Longitude	52.84	51.80	51.73	51.30
Latitude	36.07	36.20	36.38	36.23
Time series	01/01/2003-30/09/2020	01/01/2006-30/09/2020	01/01/2006-30/09/2020	01/01/2001-30/09/2020
Observations (Months)	213	175	175	237
R^2	0.956	0.946	0.972	0.956
Adjusted R^2	0.956	0.946	0.972	0.956
MSE	2.426	3.062	1.276	2.426
RMSE	1.557	1.750	1.130	1.557
MAPE	44.598	45.283	81.096	44.598
DW	1.751	1.040	1.669	1.751

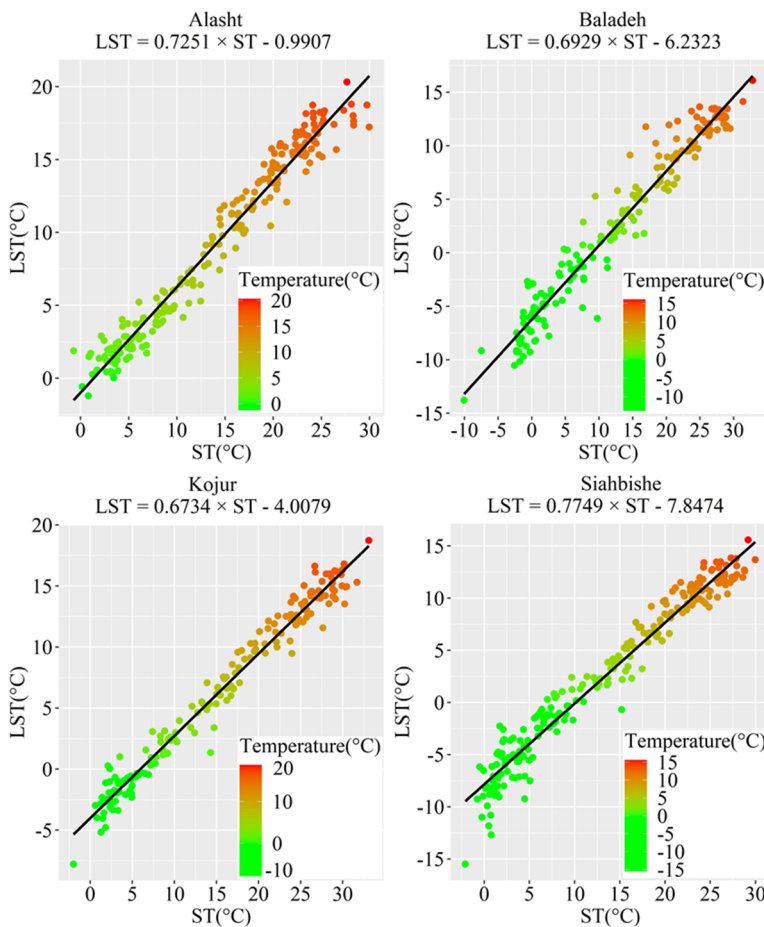


Fig. 3 Distribution of LST data relative to soil temperature (ST) values along with its linear regression equation for selected stations.

Therefore, the Mann–Kendall nonparametric test was used to analyze the trends in the nighttime LST variability. Table 5 presents the results for both the N and S aspects. The changes in the LST were averaged over all elevation levels from 1500 to 4000 m on a monthly scale. On the N aspect, the LST showed a clear increasing trend during the warm months. However, the trend was only significant (at a level of 5%) for 4 months: May (p -value = 0.006, Kendall’s τ = 0.429), June (p -value = 0.000, Kendall’s τ = 0.533), July (p -value = 0.000, Kendall’s τ = 0.676), and September (p -value = 0.016, Kendall’s τ = 0.381). On the S aspect, the LST showed a decreasing trend in October, but this was not significant (p -value = 0.200, Kendall’s τ = -0.200). The LST showed an increasing trend for the other months, but the trend was only significant for August at p -value = 0.038 (Kendall’s τ = 0.038).

The Mann–Kendall nonparametric test was used to analyze the LST difference between the N and S aspects at the same elevation level on a monthly

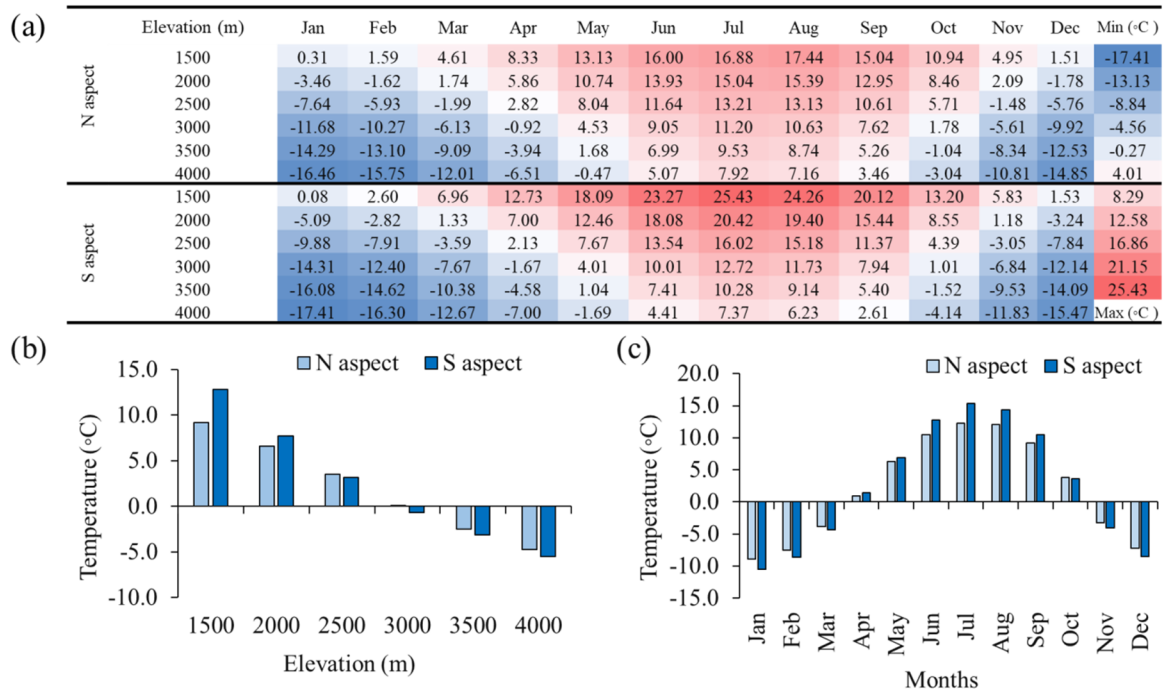


Fig. 4 Average LSTs on the N and S aspects: (a) monthly average at different elevation levels, (b) annual average at different elevation levels, and (c) monthly average across all elevation levels.

scale. Table 6 presents the results. The LST difference between the N and S aspects showed a decreasing trend from October to April, but this trend was only significant for 2 months: January (p -value = 0.043, Kendall's τ = -0.324) and February (p -value = 0.009, Kendall's τ = -0.410). The LST difference showed an increasing trend from May to September, and this trend was significant for May (p -value = 0.001, Kendall's τ =0.514), June (p -value = 0.004, Kendall's τ = 0.448), and July (p -value = 0.027, Kendall's τ = 0.352).

3.1.3 Decadal trends

The study covered a 20-year period (2000–2021),

so the changes in the LST between the two decades were also analyzed. The monthly average LST showed its largest decadal decrease of -1.48°C at the elevation level of 4000 m on the N aspect in March and its largest decadal increase of 2.7°C at the elevation level of 1500 m on the N aspect in July (Fig. 5a). For both the N and S aspects, the monthly average LST showed a decadal decrease in autumn (October–November) and at the end of winter (March). The monthly average LST showed a decadal decrease in February for the N aspect but showed a decadal increase for the S aspect (Fig. 5c). For the N aspect, the largest decadal increases in the monthly average LST were in July (1.58°C), June (1.48°C), and May (1.40°C), and the largest decadal

Table 5 Trends of the monthly average LST for the N and S aspects based on the Mann–Kendall nonparametric test

Aspect	Variable	Min.	Max.	Mean	Standard deviation	Kendall's tau	p -value (Two-tailed)	Sen's slope:
N aspect	Jan	-14.312	-5.898	-8.870	2.113	-0.010	0.976	-0.008
	Feb	-11.042	-4.939	-7.512	1.799	-0.010	0.976	-0.006
	Mar	-8.164	0.257	-3.812	2.136	0.029	0.882	0.009
	Apr	-2.478	3.555	0.939	1.715	-0.029	0.882	-0.025
	May	3.422	8.794	6.277	1.410	0.429	0.006*	0.148
	Jun	8.463	13.512	10.447	1.350	0.533	0.000*	0.156
	Jul	10.249	15.231	12.297	1.245	0.676	0.000*	0.150
	Aug	10.498	14.589	12.121	0.937	0.114	0.493	0.029
	Sep	6.948	10.691	9.158	0.925	0.381	0.016*	0.078
	Oct	2.166	5.967	3.803	1.154	-0.257	0.111	-0.069
	Nov	-7.711	-0.497	-3.198	1.621	-0.133	0.421	-0.047
	Dec	-11.531	-3.711	-7.221	2.202	0.143	0.387	0.084
S aspect	Jan	-17.251	-5.869	-10.44	2.384	0.314	0.314	0.049
	Feb	-13.717	-4.372	-8.574	2.157	0.190	0.190	0.244
	Mar	-8.102	0.081	-4.336	2.160	0.076	0.076	0.655
	Apr	-3.007	4.622	1.436	1.980	0.267	0.267	0.098
	May	4.467	8.869	6.930	1.175	0.343	0.343	0.031
	Jun	9.221	14.837	12.786	1.257	0.352	0.352	0.027
	Jul	13.257	17.249	15.374	1.215	0.267	0.267	0.098
	Aug	12.803	16.078	14.333	0.781	0.038	0.038*	0.835
	Sep	8.428	11.904	10.480	0.946	0.324	0.324	0.043
	Oct	1.870	5.711	3.584	1.196	-0.200	0.200	0.220
	Nov	-9.128	-1.681	-4.043	1.606	0.152	0.152	0.355
	Dec	-13.266	-3.422	-8.540	2.617	0.352	0.352	0.027

Table 6 Trends of the LST difference between the N and S aspects based on the Mann–Kendall nonparametric test

Variable	Min.	Max.	Mean	Standard deviation	Kendall's τ	p -value (Two-tailed)
Jan	-4.635	3.116	1.577	1.947	-0.324	0.043*
Feb	-1.636	2.675	1.062	1.068	-0.410	0.009*
Mar	-0.705	1.920	0.524	0.652	-0.305	0.057
Apr	-5.270	0.766	-0.497	1.538	-0.105	0.532
May	-1.366	0.411	-0.653	0.531	0.514	0.001*
Jun	-3.696	-0.758	-2.339	0.748	0.448	0.004*
Jul	-4.764	-0.965	-3.077	1.040	0.352	0.027*
Aug	-3.953	0.145	-2.213	0.995	0.114	0.493
Sep	-2.182	-0.112	-1.322	0.490	0.105	0.532
Oct	-0.856	1.547	0.219	0.537	-0.152	0.355
Nov	-2.250	1.963	0.845	1.087	-0.219	0.178
Dec	-3.361	2.959	1.319	1.693	-0.257	0.111

Note: *significance level of 5%.

decrease was in March (-1.23°C). For the S aspect, the largest decadal increases in the monthly average LST were in January (1.88°C) and December (1.53°C), and the largest decadal increase was in October (-0.75°C). The annual average LST showed a decadal increase at all elevation levels, but the intensity varied with the elevation level (Fig. 5b). Across all elevation levels, the annual average LST showed a larger decadal increase

on the S aspect (0.60°C) than on the N aspect (0.37°C).

Fig. 6 shows the spatial patterns of the decadal changes in the annual average LST of the N and S aspects and compares them with the topography. At elevation levels of 2000 m and higher, the decadal changes in the annual average LST were greater on the S aspect than on the N aspect. The decadal change in the annual average LST showed the smallest difference

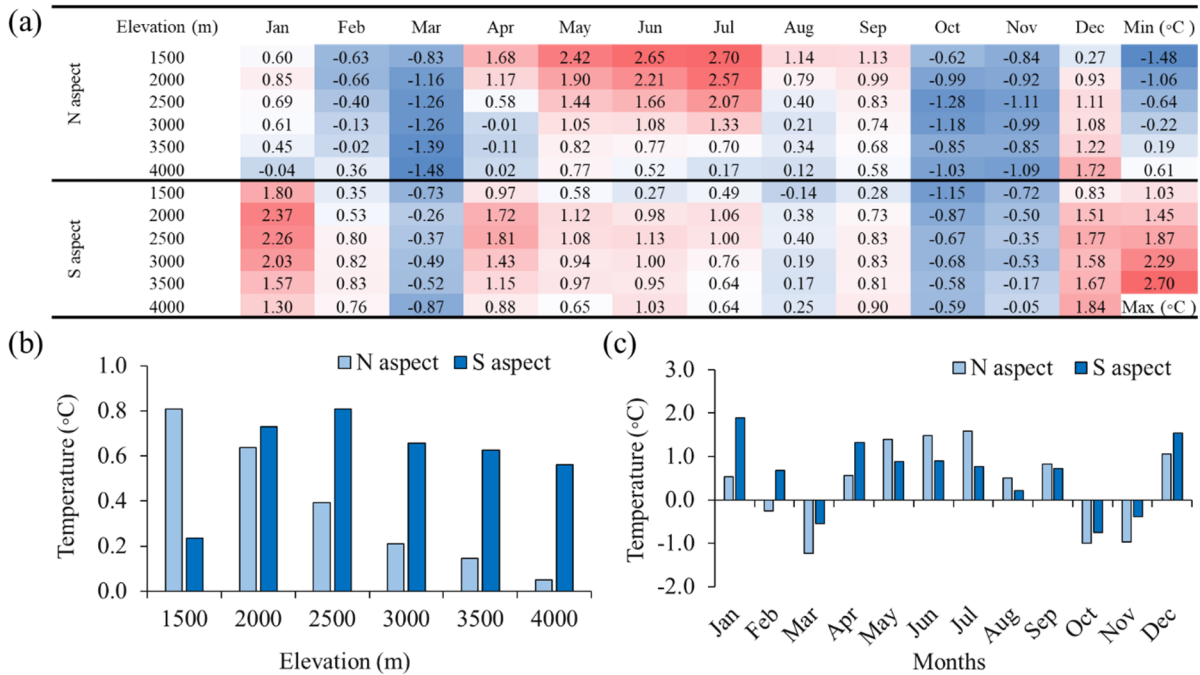


Fig. 5 Decadal changes in the average LSTs of the N and S aspects: (a) monthly average at different elevation levels, (b) annual average at different elevation levels, and (c) monthly average across all elevation levels.

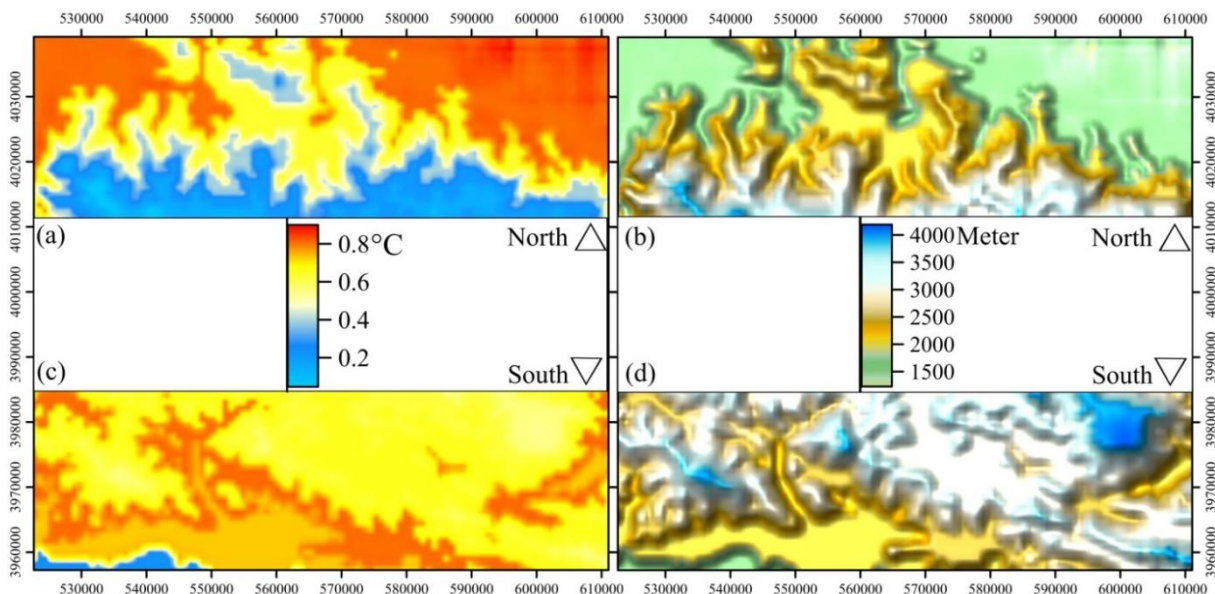


Fig. 6 Spatial patterns of the decadal changes in the annual average LST for the (a) N aspect and (c) S aspect; topographies of the (b) N aspect and (d) S aspect.

between the N and S aspects at an elevation level of 2000 m (0.09°C) and the largest difference at an elevation level of 1500 m (0.57°C). The difference between the N and S aspects increased with elevation.

3.2 Changes in the lapse rate

The lapse rate is defined as the decrease in temperature with increasing elevation, which is important in meteorology, especially in the troposphere, because it is used to determine how quickly water vapor in the air condenses into clouds. Climate change can affect the spatiotemporal patterns of the lapse rate. Thus, the spatiotemporal variability of the lapse rate was investigated for the study area. Fig. 7a shows that the LST decreased with increasing elevation for all months and elevation levels. Based on the annual average LST, the lapse rate across the entire elevation range was greater on the S aspect at -3.75°C ($-0.75^{\circ}\text{C}/100\text{ m}$) than on the N aspect at -2.78°C ($-0.56^{\circ}\text{C}/100\text{ m}$). The lapse rate fluctuated from a minimum of -1.33°C between 4000 and 3500 m on the S aspect in January to a maximum of -5.73°C between 2000 and 1500 m on the N aspect in April. For the N aspect, the minimum lapse rate was from mid-spring to late summer. For the S aspect, the minimum lapse rate was from the end of autumn to the middle of winter. For the S aspect, the lapse rate changed more slowly above elevation levels of 3000 m, and a similar pattern was observed for the N aspect, especially in

autumn and winter (Fig. 7b, 7c). At the same elevation level, the difference in the lapse rate between the N and S aspects was greater in the warm months than in the cold months. The largest differences in the lapse rate were observed in July (1.81°C), June (1.58°C), and August (1.55°C). The smallest differences in the lapse rate were observed in December (0.12°C) and January (0.14°C) (Fig. 7c).

Fig. 8 shows the spatial patterns for the lapse rate according to the annual average LST (Fig. 8a, c) and compares them with the topography (Fig. 8b, d). The smallest differences between the lapse rates of the N and S aspects were 0.04°C at the elevation levels of 3000–3500 m and 0.18°C at the elevation levels of 3500–4000 m. The largest difference was 2.50°C at 1500–2000 m. Table 7 presents the trends of the lapse rate based on the monthly average LST for the N and S aspects, which were obtained by the Mann–Kendall nonparametric test. The N aspect showed a decreasing trend for the lapse rate for most months of the year, and this trend was significant for April–July. The S aspect also showed a decreasing trend for the lapse rate in the late spring and summer, but the trend was not significant for any months.

3.3 Comparison of spatial changes in the moisture regime across studied elevation levels

The analysis of the spatial variations in TWI reveals that, for the northern aspect, the average

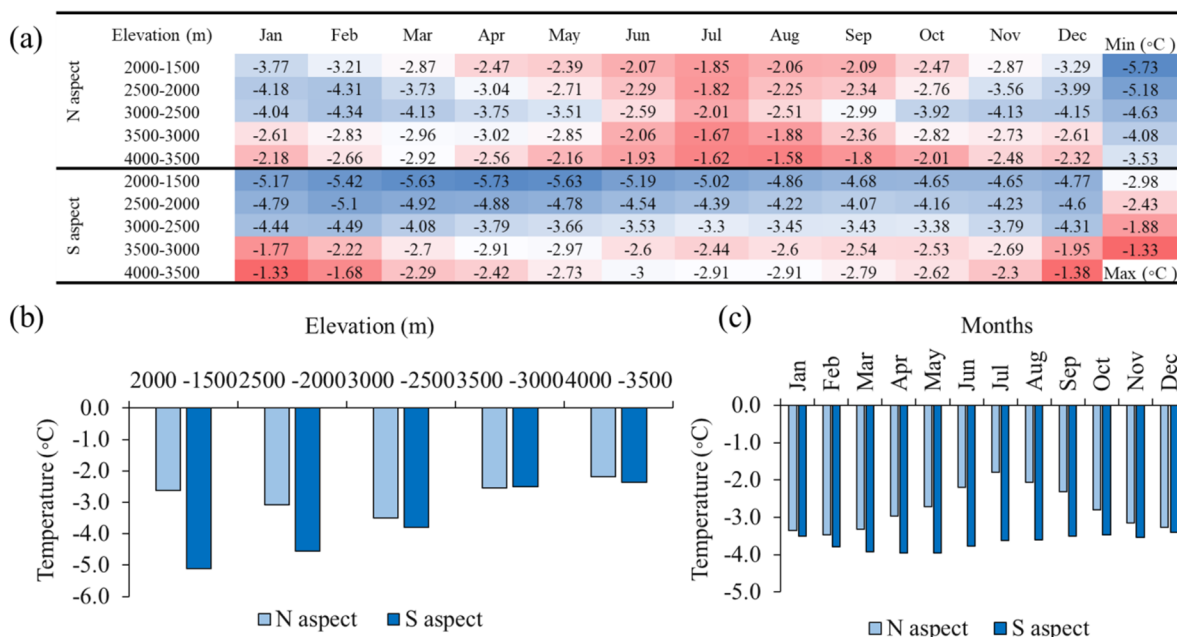


Fig. 7 Lapse rates for the N and S aspects: (a) based on the monthly average LST for different elevation levels, (b) based on the annual average LST for different elevation levels, (c) and based on the monthly average LST across all elevation levels.

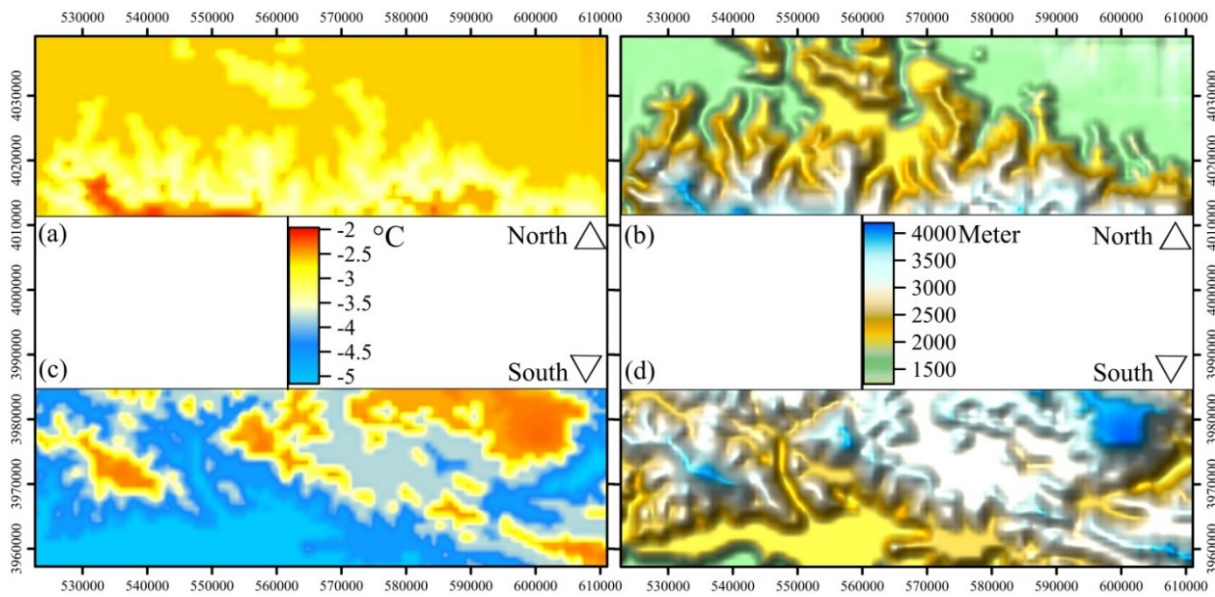


Fig. 8 Spatial patterns of the lapse rate based on the annual average LST for the (a) N aspect and (c) S aspect; topography of the (b) N aspect and (d) S aspect.

Table 7 Trends of the lapse rate for the N and S aspects based on the results of the Mann–Kendall nonparametric test

Aspect	Variable	Min. (°C)	Max. (°C)	Mean (°C)	Standard deviation	Kendall's τ	p-value (Two-tailed)	Sen's slope
N aspect	Jan	-3.807	-3.008	-3.354	0.234	-0.190	0.244	-0.013
	Feb	-3.881	-2.886	-3.468	0.299	0.133	0.421	0.012
	Mar	-4.141	-2.902	-3.323	0.384	-0.257	0.111	-0.023
	Apr	-3.861	-2.163	-2.967	0.389	-0.333	0.037*	-0.021
	May	-4.004	-2.137	-2.721	0.358	-0.362	0.023*	-0.020
	Jun	-3.868	-1.520	-2.187	0.479	-0.438	0.005*	-0.029
	Jul	-3.962	-0.839	-1.793	0.618	-0.381	0.016*	-0.044
	Aug	-3.631	-1.303	-2.063	0.492	-0.133	0.421	-0.017
	Sep	-3.643	-1.952	-2.317	0.344	-0.086	0.613	-0.004
	Oct	-3.491	-2.262	-2.796	0.246	-0.114	0.493	-0.006
	Nov	-3.639	-2.736	-3.153	0.227	-0.029	0.882	-0.002
	Dec	-3.901	-2.795	-3.273	0.306	0.248	0.126	0.022
S aspect	Jan	-4.174	-3.002	-3.499	0.244	0.010	0.976	0.000
	Feb	-4.039	-3.329	-3.779	0.173	0.143	0.387	0.006
	Mar	-4.219	-3.356	-3.926	0.208	-0.048	0.789	-0.003
	Apr	-4.621	-3.408	-3.946	0.238	-0.038	0.835	-0.001
	May	-4.194	-2.971	-3.956	0.245	-0.133	0.421	-0.005
	Jun	-4.054	-2.194	-3.771	0.374	0.124	0.456	0.004
	Jul	-3.921	-2.051	-3.612	0.388	-0.095	0.572	-0.005
	Aug	-3.850	-2.384	-3.610	0.299	-0.200	0.220	-0.005
	Sep	-3.770	-1.783	-3.503	0.402	0.057	0.744	0.001
	Oct	-3.731	-2.603	-3.468	0.227	0.067	0.699	0.002
	Nov	-3.956	-2.998	-3.532	0.219	0.219	0.178	0.009
	Dec	-3.767	-3.023	-3.401	0.206	0.276	0.086	0.017

Note: *significance level of 5%.

threshold of this index ranges from a minimum of 3.22 to a maximum of 16.20. In contrast, for the southern aspect, the minimum and maximum values range from 2.93 to 16.90, respectively. Fig. 9 illustrates that the maximum TWI in the northern aspect is distributed from the center to the west, while in the southern

aspect, the maximum TWI extends from the center to the east. In this study, TWI is categorized into five levels. The first class, representing the lowest moisture content, is classified as dry. The dry class covers 24.9% of the northern slope area and 32.4% of the southern slope area. Except for the dry class, the research results

indicate that the area of other classes, signifying increased humidity, is larger for the northern slope compared to the southern slope.

The largest area is allocated to the relatively dry class, constituting 40.9% for the northern slope and 38.8% for the southern slope. For the moderately wet class, the area percentages in the northern and southern slopes are 23.5% and 21.4%, respectively. The very wet class covers 8.9% of the northern slope and 5.9% of the southern slope. Furthermore, the extreme wet class occupies 1.7% of the northern slope area, while for the southern slope, its area is 1.5%. In this section, changes in the spatial distribution of TWI were assessed and compared across various elevation levels

for the two study areas. Analyzing TWI spatial variations reveals that, for the northern slope, the maximum extent of dry areas is observed at elevation levels of 1500 m a.s.l. (50.7%) and 2000 m a.s.l. (43.6%). Conversely, the southern slope exhibits the minimum extent of the dry class at the altitude level of 1500 m a.s.l. (4.9%). Overall, the frequency of the dry class at different altitude levels is higher in the southern slope compared to the northern slope. In the northern slope, the frequency of very wet and extreme wet classes increases with elevation, whereas in the southern slope, the peak frequency of these classes is first encountered at 2500 m a.s.l. and then at 1500 m a.s.l. (Fig. 10).

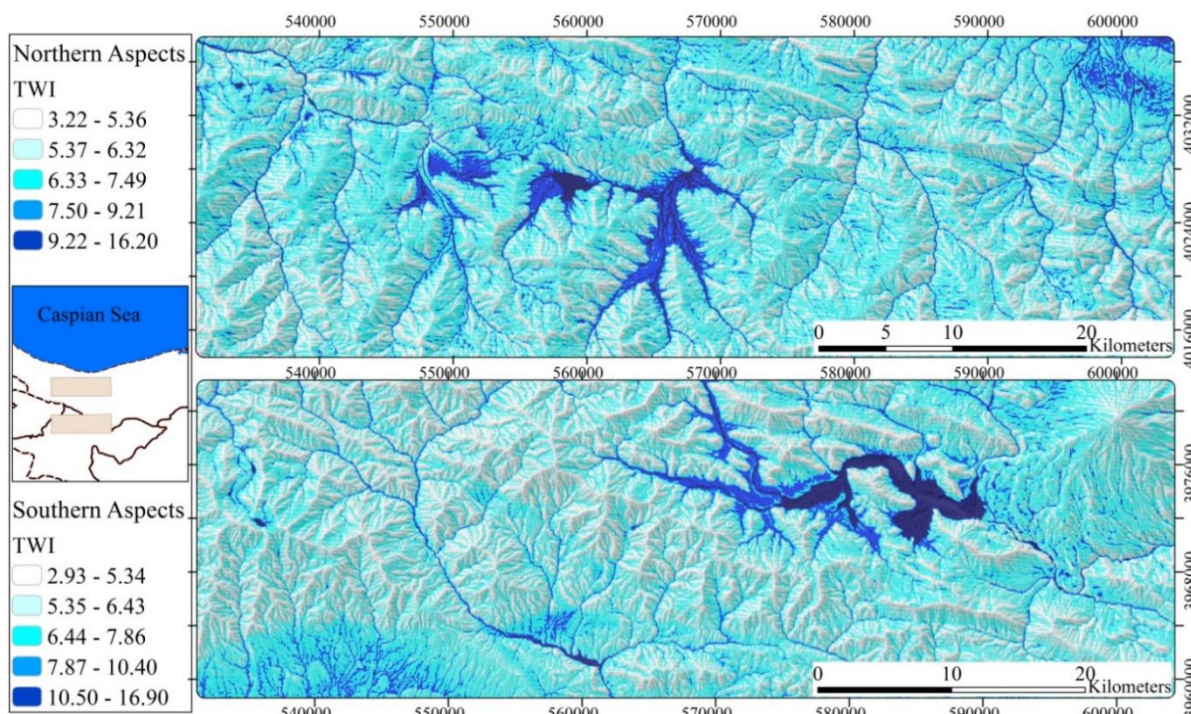


Fig. 9 Spatial changes of the TWI values in the N and S aspects.

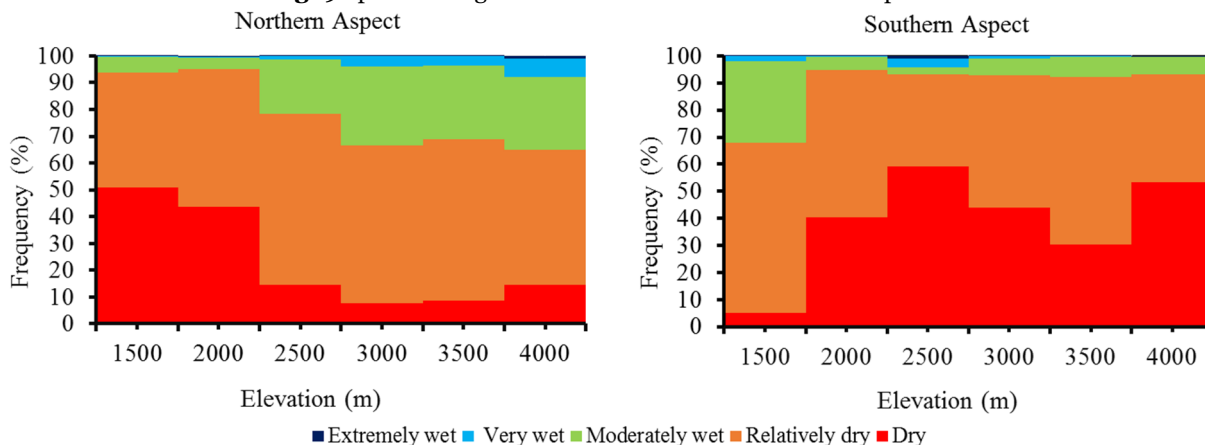


Fig. 10 Comparison of the percentage frequency of TWI classes in different altitude levels for the northern and southern slopes.

These findings align well with the spatial LST pattern changes across altitude levels for both slopes. Fig. 4b, comparing the average LST for various altitude levels in the northern and southern slopes, indicates that at lower levels of the northern slope, the LST is lower than in the southern slope. However, as the altitude increases, the average LST in the northern slope surpasses that of the southern slope. This pattern precisely corresponds to the changes in TWI. In the northern slope, the largest extent of the dry (wet) class is observed at lower (higher) levels. Conversely, for the southern slope, the maximum extent of the dry (wet) class is observed at higher (lower) levels. This illustrates a clear agreement between the spatial distribution of TWI and LST. Essentially, this suggests that the moister regime can be both influential and impacted factors in the LST transformation of the study area. Consequently, it is anticipated that changes in LST due to global warming can influence the moister and hydrological pattern of the region. To substantiate this hypothesis, a new and comprehensive study is required, considering various indicators, objectives, and evaluation methods.

3.4 Assessment of land use changes in the study area over the last two decades

In this investigation, land use changes were examined using the six classes outlined in Table 2. The data indicates that forests cover 44.88% of the northern slope, while the southern slope exhibits no extent of this land use. Among the various uses in the northern slope, grasslands dominate with 52.15%, while urban and built-up lands and non-vegetated lands are the least prevalent, each occupying only 0.12% of the area. In the southern slope, shrublands and croplands have the smallest areas at 0.02% and 0.03%, respectively, while grasslands cover the largest portion with 90.19% (Table 8).

The average decade-wise changes for each land

use were assessed at this stage. In the northern slope, all land uses, except grasslands (with an increase of 1758.42 ha/decade) and non-vegetated lands (with an increase of 60.12 ha/decade), witnessed a reduction in area. The most significant decline occurred in croplands, experiencing a rate of -969.89 ha/decade. It is noteworthy that, except for forests ($r=-0.20$) and urban and built-up lands ($r=-0.27$), whose change trends are not significant, the trend for other land uses is significant at the 95% confidence level (Table 8).

In the southern slope, similar to the northern slope, the grasslands land use has experienced an increasing trend, with average decadal changes reaching 1996.17 hectares. Unlike the northern slope, urban and built-up lands have also shown an increasing trend, with changes of 169.32 ha/decade. However, other land uses have witnessed decreasing decade-wise changes. Notably, non-vegetated lands exhibited the most rapid decline among other uses, decreasing by -2078.46 ha/decade. Conversely, this land use has seen an increase in the northern slope. In the southern slope, grasslands and urban and built-up lands exhibited significant increasing changes with $r=0.87$ and $r=0.92$, respectively, at the 99% confidence level. Conversely, shrublands ($r=-0.42$) and non-vegetated lands ($r=-0.90$) experienced significant decreasing changes at the 99% confidence level. No significant trend was observed for other land uses (Table 8).

In the final step of this research segment, the correlation between the variability of different land uses and LST was examined (annual average extracted from all elevation levels). Among these, only a significant relationship (at the 95% confidence level) was identified between LST changes and urban and built-up lands use. The correlation coefficient ($r=0.44$) was for the northern slope and $r=0.64$ for the southern slope (Table 9). This suggests that an increase in the area associated with urban and built-up lands corresponds to an increase in the annual average LST, which is logically plausible. Although an inverse

Table 8 Total average of frequency percentage for different land uses. Evaluation of the significant trend (r) for the average decadal changes in the area (ha) of LULCs during the study period for both northern and southern slopes.

LULC	N aspect			S aspect		
	Area (%)	ha/decade	r	Area (%)	ha/decade	r
Forests	44.88	-265.52	-0.20	0.00	0.00	0.00
Shrublands	0.42	-547.07	-0.45*	0.02	-328.26	-0.42*
Grasslands	52.15	1758.42	0.42*	90.19	1996.17	0.87**
Croplands	2.31	-969.89	-0.43*	0.03	7.77	0.16
Urban and built-up Lands	0.12	-11.42	-0.27	6.03	169.32	0.92**
Non-vegetated lands	0.12	60.12	0.49*	3.72	-2078.46	-0.90**

Notes: * and ** indicate significance levels of 5% and 1%, respectively.

relationship with LST is observed for non-vegetated lands, this correlation is not significant but approaches a significant level.

Table 9 Correlation between annual mean LST variability and LULCs for the northern and southern aspects. (* indicate significance levels of 5%)

LULCs	N	S
Forests	-0.10	0.00
Shrublands	-0.25	0.28
Grasslands	0.13	0.30
Croplands	0.11	-0.17
Urban and Built-up Lands	0.44*	0.64*
Non-Vegetated Lands	-0.35	-0.38

4 Discussion

The monthly average LST was found to be lower for the warm seasons of the year (spring and summer) on the N aspect than on the S aspect while the opposite was true for the cold seasons. In the summer, most of Iran is under the influence of high-pressure warm systems due to the Azores High that bring hot and dry air from the south (Roshan et al. 2020; Lashkari et al. 2020). However, the N aspect is less affected by these warm systems, and atmospheric precipitation during this period can reduce the LST (Scherrer et al. 2012; Alijani 2002). During the cold seasons, factors such as the higher humidity, the water zone of the Caspian Sea, and the greater vegetation cover of the N aspect work together to increase the LST more for the N aspect than for the S aspect (Alijani 2002). The annual average LST was lower for the N aspect at low elevation levels (2000 m and below) and was lower for the S aspect at high-elevation levels (greater than 2000 m). At low elevations, these results may be because most of the atmospheric precipitation was on the N aspect rather than on the S aspect. At high elevations, the amount of atmospheric precipitation was reduced for both aspects and thus had a smaller effect on the LST difference. The S aspect has a less dense vegetation cover because it is dryer, so it experiences a greater decrease in the LST at night because more energy is released. This process is more intense at higher elevations, which may explain why the LST was lower on the S aspect than on the N aspect.

One of the outcomes of this study is the revelation of the influence of the LST change pattern corresponding to variations in the moisture regime across different altitude levels in both aspects of the Alborz Mountains. In the northern slope, the

predominant dry (wet) class is found at lower (higher) elevations, while in the southern slope, it is observed at higher (lower) elevations. Consequently, this spatial moisture pattern results in a lower (higher) annual average LST for the northern slope compared to the southern slope at low (higher) altitude levels. Additionally, changes in land use have been identified to impact the emergence of distinct spatial LST patterns. Notably, the frequency and changing trends of land uses differ between the two mountain aspects over the last two decades. Furthermore, the findings reveal that, among the examined LULC categories, a direct and significant relationship (at a 95% confidence level) exists between LST changes and the urban and built-up lands use.

The difference in the monthly average LST between the N and S aspects decreased for the cold months and increased for the warm months. One of the factors that affect the LST difference is the type of atmospheric precipitation, especially snowfall during the cold months. The increased snowfall on the N aspect increases the albedo, which in turn should decrease the LST. However, some studies (Naghizadeh et al. 2019; Shahnaz et al. 2023; Yang et al. 2022; Barnett et al. 2005), have shown that climate change has increased the elevation of the snowline. The increased elevation of the snowline allows a larger area of the N aspect to absorb heat and experience an increase in LST. Therefore, the increased elevation of the snowline on the N aspect can explain the decrease in the LST difference between the N and S aspects during the cold months. Various studies have shown that changes in land use have decreased the forest cover of the N aspect over the last few decades (Mirzayi et al. 2013; Jahanifar et al. 2020; Alchin and Darvishsefat 2023). Vegetation reduces the reflection of solar energy at night and prevents the LST from decreasing. Thus, the reduced forest cover has increased the reflection of solar energy on the N aspect. Meanwhile, the S aspect receives more energy during the summer, which increases the LST difference during this time.

The lapse rate decreased more for the S aspect than the N aspect. The water zone of the Caspian Sea and the higher density of vegetation cover may have helped mitigate the decrease in the lapse rate on the N aspect compared to the S aspect. For the N aspect, the lapse rate was smaller during the hot months than during the cold months. These results may be explained by the reduced diversity of atmospheric systems during the hot months, more stable

atmospheric conditions owing to the pressure of the Azores High, increasing length of the day, and more uniformity in the radiation distribution. The S aspect showed a slight difference in that the largest decrease in the lapse rate took place during autumn, followed by during the summer.

Researchers use MODIS data and the Mann-Kendall test to identify climate dynamics patterns and differences across continents. Jiménez-Muñoz et al. (2013) calculated the rate of warming in the Patagonian Sub-Antarctic Forest by the Mann-Kendall test and Sens's slope on time-series images of MODIS monthly LST. They found that the warming rate was 0.78 and 0.33°C/decade. The warming trends in South America (Peru, Bolivia, and Chile) and the Purog Kangri ice field, Qinghai-Tibetan Plateau, were mapped by Aguilar-Lome et al. (2019) and Qie et al. (2020). using the Mann-Kendall test and Sens's slope on the time series of MODIS 8-day (2000–2017) and daily (2001–2018) at 1 km, respectively. Hassan et al. (2021) utilized MODIS-derived LST data and employed the Mann-Kendall test to examine the influence of climate change on ecosystems in the 21 natural subregions of Alberta. The results indicate a rapid increase in temperature, which is impacting the distribution of plants and generating concerns about the decline of biodiversity in the area. These collective efforts highlight the universal applicability of this research methodology.

Analyses of the lapse rates for other mountain ranges have also reveal striking seasonal and spatial differences. The Sierra Nevada has a lapse rate of 5.8°C/km (Dobrowski et al. 2009), while the Cascades have smaller lapse rates of 4.9°C/km (Minder et al. 2018) and 4°C/km (O'Neal et al. 2010). The Colorado Rockies and Yellowstone National Park have lapse rates of 4.1°C/km in winter and 6.2°C/km in summer (Huang et al. 2008). The regional differences in lapse rates indicating the importance of understanding the local changes in the LST with elevation and vegetation cover (Pepin and Seidel 2005).

Our study of LST trends using MODIS data and the Mann-Kendall test aims to contribute to mountain climate discourse and demonstrate the universality of our findings. By comparing our data to other mountain climate studies, we find trends that transcend geographical boundaries and improve the generalizability of our research.

The spatial patterns of the lapse rate according to the annual average LST (Fig. 8a, c) indicate that the

lapse rate decreased with increasing elevation. One of the factors may be the decreased diversity of land use at higher elevations. At lower elevations, more land uses are possible, which can increase the lapse rate. Meanwhile, climate change may explain the significant decrease in the lapse rate for the months of April–July. Overall, the spatial trends indicate that the LST difference has decreased at different elevation levels for these months.

Previous studies have shown that climate change has caused atmospheric precipitation at higher elevation levels to shift from solid (snow) to liquid (rain), which not only increases the elevation of the snowline but also reduces the amount of water reserves in the form of snowpack (Howarth and Painter 2016; Yan et al. 2016; Chen et al. 2022). These changes in the rainfall regime can also affect the risk of flooding (López-Tarazón et al. 2019; Vuille and Bradley 2000). The Alborz Mountains have long been a tourist destination, both in winter for winter sports and in summer to escape from the heat in the lowlands (Mokhtarian et al. 2022; Akbarian Ronizi et al. 2016). However, the increased LST and decreased snowfall can threaten winter tourism in this region, similar to how climate change has threatened winter tourism in other areas around the world (Wang et al. 2022; Willibald et al. 2021). The decadal changes in the LST were found to be more severe on the S aspect than on the N aspect. Because the S aspect is drier than the N aspect, the increased LST, which is associated with a decrease in rainfall intensity, increases the desertification potential of this region. In recent years, some dust centers have appeared in Iran with various environmental consequences, including human health. This study also showed that the lapse rate has decreased across elevation levels, which can be attributed to climate change and which has also been observed in other mountainous areas (Sambuco et al. 2020; Pepin et al. 2015; Loarie et al. 2009; Burrows et al. 2014). The reduced lapse rate can limit biodiversity by reducing the amount of suitable habitat for different species, which can threaten their survival if they are unable to adapt to the new environmental conditions.

5 Conclusion

The LST showed a significant increasing trend for the warm months (May to August), which may have negative environmental consequences. In most of Iran,

the hot months are associated with a decrease in atmospheric precipitation, which increases the demand for water. An increase in LST during this period increases the evaporation potential and thus can lead to water insecurity. In summary, the increased LST and decreased lapse rate of the Central Alborz Mountains have important consequences for the surrounding area in terms of biodiversity, water resources, flood risk, winter tourism, and even forest fires due to the expansion of the dry season. The climatic patterns of this region are the result of complex interactions between local and extra-local components such as the Caspian Sea, topography, forest cover, western wind system, Siberian high pressure, and deserts. Changes to any of these components due to climate change, such as a decrease in the intensity of the Siberian high pressure, increases in the evaporation potential and water temperature of the Caspian Sea, shifts in the western wind system, and even local factors such as changes in land use will affect the climatic patterns of this region. This study only focused on the changes to the LST, which is affected by the interaction of different components. Future studies will focus on considering the effect of each of these components on the LST independently.

Simultaneously, a range of measures is proposed for enhanced climate change management in the West Middle Alborz region. Firstly, the implementation of intelligent water resource management policies is crucial to mitigate the impacts of rising temperatures and drought during the warmer seasons. Secondly, the adoption of sustainable agricultural technologies serves as a pivotal tool to alleviate pressure on water resources while preserving soil and natural ecosystems. The promotion of sustainable tourism is another avenue to safeguard the environment, boost regional economic growth through informed tourism management, and mitigate adverse effects of climate change on the local tourism industry. Recognizing the direct link between climate change and heightened fire risks in forested areas, the construction of drainage structures and the implementation of fire warning systems can form a risk management strategy to control or mitigate risks associated with extended dry seasons. Attracting investments in environmental protection and climate change projects through incentives and facilitations can foster sustainable development and resilience to climate change in the region. Moreover, increased research in meteorology, biology, and environmental engineering is imperative

for a more precise understanding and effective planning in climate change adaptation and mitigation efforts.

Acknowledgments

Open access funding provided by University of Szeged. The authors declare that no funds, grants, or other support were received during the preparation of this manuscript.

Author Contribution

ROSHAN Gholamreza: Conceptualization, Methodology, writing-original draft preparation, Software. SARLI Reza: Conceptualization, Data Acquisition, Visualization, Software. GHANGHERMEH Abdolazim: Analysis, Writing-Reviewing and Editing, Supervision. TAHERIZADEH Mehrnoosh: Contributed to the writing, Analysis, Writing- Reviewing and Editing. NIKNAM Arman: Discussion, Resources, Writing Editing and Reviewing, Supervision.

Ethics Declaration

Availability Of Data/Materials: Data supporting this Research article are available from the corresponding author on request.

Conflict of interest: The authors declare no conflicts of interest.

Open Access

This article is licensed under a Creative Commons Attribution 4.0 International License, which permits use, sharing, adaptation, distribution and reproduction in any medium or format, as long as you give appropriate credit to the original author(s) and the source, provide a link to the Creative Commons licence, and indicate if changes were made. The images or other third party material in this article are included in the article's Creative Commons licence, unless indicated otherwise in a credit line to the material. If material is not included in the article's Creative Commons licence and your intended use is not permitted by statutory regulation or exceeds the permitted use, you will need to obtain permission directly from the copyright holder. To view a copy of this licence, visit <http://creativecommons.org/licenses/by/4.0/>.

References

- Abe S (2013) Conceptions of nature in Iran: science, nationalism, and heteroglossia. *J Anthropol Res* 69(2): 201-223. <https://doi.org/10.3998/jar.0521004.0069.203>
- Aguilar-Lome J, Espinoza-Villar R, Espinoza JC, et al. (2019) Elevation-dependent warming of land surface temperatures in the Andes assessed using MODIS LST time series (2000-2017). *Int J Appl Earth Obs Geoinf* 77:119-128. <https://doi.org/10.1016/j.jag.2018.12.013>
- Akbarian Ronizi SR, Roshan GHR, Negahban S (2016) Assessment of tourism climate opportunities and threats for villages located in the northern coasts of Iran. *Int J Environ Res* 10:601-612.
- Alchin AA, Darvishsefat AA (2023) Investigating the trend of vegetation changes(Greening and Browning) using MODIS-NDVI time series in Mazandaran Province. *Wood Sci Technol* 30(1): 125-140. <https://doi.org/10.22069/JWFST.2023.20755.1991>
- Alijani B (2002) Variations of 500 hPa flow patterns over Iran and surrounding areas and their relationship with the climate of Iran. *Theor Appl Climatol* 72:41-54. <https://doi.org/10.1007/s007040200011>
- Arsalani M, Grieflinger J, Bräuning A (2022) Tree-ring-based seasonal temperature reconstructions and ecological implications of recent warming on oak forest health in the Zagros Mountains, Iran. *Int J Biometeorol* 66:2553-2565. <https://doi.org/10.1007/s00484-022-02380-5>
- Asakereh H, Ashrafi S (2023) An investigation into trends in frequency and proportion of different durations of various types of extreme precipitation in Iran. *Meteorol Appl* 30:1-17. <https://doi.org/10.1002/met.2117>
- Azizi G, Arsalani M, Bräuning A, et al. (2013) Precipitation variations in the central Zagros Mountains (Iran) since A.D. 1840 based on oak tree rings. *Palaeogeogr Palaeoclimatol Palaeoecol* 386:96-103. <https://doi.org/10.1016/j.palaeo.2013.05.009>
- Barnett TP, Adam JC, Lettenmaier DP (2005) Potential impacts of a warming climate on water availability in snow-dominated regions. *Nature* 438: 303-309. <https://doi.org/10.1038/nature04141>
- Baumann M, Radeloff VC, Avedian V, et al. (2015) Land-use change in the Caucasus during and after the Nagorno-Karabakh conflict. *Reg Environ Chang* 15:1703-1716. <https://doi.org/10.1007/s10113-014-0728-3>
- Beven KJ, Kirkby MJ (1979) A physically based, variable contributing area model of basin hydrology. *Hydrol Sci Bull* 24: 43-69. <https://doi.org/10.1080/02626667909491834>
- Bonshoms M, Ubeda J, Liguori G, et al. (2022) Validation of ERA5-Land temperature and relative humidity on four Peruvian glaciers using on-glacier observations. *J Mt Sci* 19: 1849-1873. <https://doi.org/10.1007/s11629-022-7388-4>
- Bradley RS, Vuille M, Diaz HF, et al. (2006) Threats to water supplies in the tropical Andes. *Science* 312:1755-1757. <https://doi.org/10.1126/science.1128087>
- Burrows MT, Schoeman DS, Richardson AJ, et al. (2014) Geographical limits to species-range shifts are suggested by climate velocity. *Nature* 507: 492-495. <https://doi.org/10.1038/nature12976>
- Chang S, Wang Z, Mao D, et al. (2020) Mapping the essential urban land use in Changchun by applying random forest and multi-source geospatial data. *Remote Sens* 12(15): 2488. <https://doi.org/10.3390/RS12152488>
- Chaplot V, Walter C, Curmi P (2000) Improving soil hydromorphy prediction according to DEM resolution and available pedological data. *Geoderma* 97: 405-422. [https://doi.org/10.1016/S0016-7061\(00\)00048-3](https://doi.org/10.1016/S0016-7061(00)00048-3)
- Chen Z, Zhu R, Yin Z, et al. (2022) Hydrological response to future climate change in a mountainous watershed in the Northeast of Tibetan Plateau. *J Hydrol Reg Stud* 44: 101256. <https://doi.org/10.1016/j.ejrh.2022.101256>
- Colombi A, De Michele C, Pepe M, et al. (2007) Estimation of daily mean air temperature from MODIS LST in alpine areas. *EARSel eProceedings* 6: 38-46.
- Diaz HF, Bradley RS (1997) Temperature variations during the last century at high elevation sites. *Clim Change* 36: 253-279. <https://doi.org/10.1023/a:1005335731187>
- Didari S, Norouzi H, Zand-Parsa S, et al. (2017) Estimation of daily minimum land surface air temperature using MODIS data in southern Iran. *Theor Appl Climatol* 130: 1149-1161. <https://doi.org/10.1007/s00704-016-1945-0>
- Dobrowski SZ, Abatzoglou JT, Greenberg JA, et al. (2009) How much influence does landscape-scale physiography have on air temperature in a mountain environment? *Agric For Meteorol* 149: 1751-1758. <https://doi.org/10.1016/j.agrformet.2009.06.006>
- Domonkos P, Tar K (2003) Long-term changes in observed temperature and precipitation series 1901-1998 from Hungary and their relations to larger scale changes. *Theor Appl Climatol* 75: 131-147. <https://doi.org/10.1007/s00704-002-0716-2>
- Domroes M, El-Tantawi A (2005) Recent temporal and spatial temperature changes in Egypt. *Int J Climatol* 25: 51-63. <https://doi.org/10.1002/joc.1114>
- Duan SB, Li ZL, Li H, et al. (2019) Validation of Collection 6 MODIS land surface temperature product using in situ measurements. *Remote Sens Environ* 225: 16-29. <https://doi.org/10.1016/j.rse.2019.02.020>
- Emadodin I, Reinsch T, Taube F (2019) Drought and desertification in Iran. *Hydrology* 6(3): 66. <https://doi.org/10.3390/hydrology6030066>
- Ewane BE, Lee HH (2017) Tree-ring reconstruction of streamflow for Palgong Mountain forested watershed in southeastern South Korea. *J Mt Sci* 14: 60-76. <https://doi.org/10.1007/s11629-016-3860-3>
- Freeman BG, Scholer MN, Ruiz-Gutierrez V, et al. (2018) Climate change causes upslope shifts and mountaintop extirpations in a tropical bird community. *Proc Natl Acad Sci U S A* 115: 11982-11987. <https://doi.org/10.1073/pnas.1804224115>
- Frierson DMW (2006) Robust increases in midlatitude static stability in simulations of global warming. *Geophys Res Lett* 33: 1-4. <https://doi.org/10.1029/2006GL027504>
- Frimpong BF, Koranteng A, Molkenthin F (2022) Analysis of temperature variability utilising Mann-Kendall and Sen's slope estimator tests in the Accra and Kumasi Metropolises in Ghana. *Environ Syst Res* 11: 1-13. <https://doi.org/10.1186/s40068-022-00269-1>
- Gadedjisso-tossou A, Adjegan KII (2021) Rainfall and temperature trend analysis by Mann-Kendall Test and Significance for Rainfed Cereal Yields in Northern Togo. *Sci* 3(1): 17. <https://doi.org/10.3390/sci3010017>
- Ghanghermeh A, Roshan G, Orosa JA, et al. (2019) Analysis and comparison of spatial-temporal entropy variability of tehran city microclimate based on climate change scenarios. *Entropy* 21: 13. <https://doi.org/10.3390/e21010013>
- Ghehsareh Ardestani E, Heidari Ghahfarrokhi Z (2021) Ensemble distribution modeling of *Salvia hydroangea* under future climate change scenarios in Central Zagros Mountains, Iran. *Glob Ecol Conserv* 26: e01488. <https://doi.org/10.1016/j.gecco.2021.e01488>
- Gocic M, Trajkovic S (2013) Analysis of changes in meteorological variables using Mann-Kendall and Sen's slope estimator statistical tests in Serbia. *Glob Planet Change* 100:172-182. <https://doi.org/10.1016/j.gloplacha.2012.10.014>
- Gupta A, Moniruzzaman M, Hande A, et al. (2020) Estimation of particulate matter (PM_{2.5}, PM₁₀) concentration and its variation over urban sites in Bangladesh. *SN Appl Sci* 2: 1-15. <https://doi.org/10.1007/s42452-020-03829-1>
- Haerberli W, Weingartner R (2020) In full transition: Key impacts of vanishing mountain ice on water-security at local to global scales. *Water Secur* 11: 100074. <https://doi.org/10.1016/j.wasec.2020.100074>
- Hassan QK, Ejiagha IR, Ahmed MR, et al. (2021) Remote sensing of local warming trend in alberta, canada during 2001-2020, and its relationship with large-scale atmospheric circulations. *Remote Sens* 13(17): 3441. <https://doi.org/10.3390/rs13173441>
- Heidarliou HB, Shafiee AB, Nasiri V, et al. (2023) Impact of Iran's forest nationalization law on forest cover changes over six decades: A case study of a Zagros sparse coppice oak forest. *Sensors* 23(2): 871. <https://doi.org/10.3390/s23020871>
- Howarth C, Painter J (2016) Exploring the science-policy interface on climate change: The role of the IPCC in informing local decision-making in the UK. *Palgrave Commun* 2: 16058. <https://doi.org/10.1057/palcomms.2016.58>
- Huang S, Rich PM, Crabtree RL, et al. (2008) Modeling monthly

- near-surface air temperature from solar radiation and lapse rate: Application over complex terrain in yellowstone national park. *Phys Geogr* 29: 158-178. <https://doi.org/10.2747/0272-3646.29.2.158>
- Huss M, Bookhagen B, Huggel C, et al. (2017) Towards mountains without permanent snow and ice: Mountains without permanent snow and ice Earth's Future. *Mt Without Perm Snow Ice* 5: 418-435. <https://doi.org/10.1002/efst.207>
- Huss M, Hock R (2018) Global-scale hydrological response to future glacier mass loss. *Nat Clim Chang* 8: 135-140. <https://doi.org/10.1038/s41558-017-0049-x>
- Hussain M, Mahmud I (2019) pyMannKendall: a python package for non parametric Mann Kendall family of trend tests. *J Open Source Softw* 4(39): 1556. <https://doi.org/10.21105/joss.01556>
- Jahanifar K, Amirnejad H, Mojaverian SM, et al. (2020) Land use change drivers in the Hyrcanian Vegetation Area: Dynamic simultaneous equations system with panel data approach. *Land Use Policy* 99: 104954. <https://doi.org/10.1016/j.landusepol.2020.104954>
- Jaiswal RK, Lohani AK, Tiwari HL (2015) Statistical analysis for change detection and trend assessment in climatological parameters. *Environ Process* 2: 729-749. <https://doi.org/10.1007/s40710-015-0105-3>
- Janizadeh S, Bateni SM, Jun C, et al. (2023) Potential impacts of future climate on the spatio-temporal variability of landslide susceptibility in Iran using machine learning algorithms and CMIP6 climate-change scenarios. *Gondwana Res* 124: 1-17. <https://doi.org/10.1016/j.gr.2023.05.003>
- Jiménez-Muñoz JC, Sobrino JA, Mattar C, et al. (2013) Spatial and temporal patterns of the recent warming of the Amazon forest. *J Geophys Res Atmos* 118: 5204-5215. <https://doi.org/10.1002/jgrd.50456>
- Kuhn M (1989) The Response of the equilibrium line altitude to climate fluctuations: theory and observations. In: Oerlemans, J. (eds), *Glacier Fluctuations and Climatic Change. Glaciology and Quaternary Geology*, vol 6. Springer, Dordrecht. https://doi.org/10.1007/978-94-015-7823-3_26
- Kumar PV, Bindi M, Crisci A, et al. (2005) Detection of variations in air temperature at different time scales during the period 1889-1998 at Firenze, Italy. *Clim Change* 72: 123-150. <https://doi.org/10.1007/s10584-005-5970-8>
- Lashkari H, Mohammadi Z, Jafari M (2020) Investigation on dynamical structure and moisture sources of heavy precipitation in south and south-west of Iran. *Arab J Geosci* 13(21): 1140. <https://doi.org/10.1007/s12517-020-06097-w>
- Lau WKM, Kim MK, Kim KM, et al. (2010) Enhanced surface warming and accelerated snow melt in the Himalayas and Tibetan Plateau induced by absorbing aerosols. *Environ Res Lett* 5: 025204. <https://doi.org/10.1088/1748-9326/5/2/025204>
- Li LM, Wang CY, Wen ZZ, et al. (2023) Landslide displacement prediction based on the ICEEMDAN, ApEn and the CNN-LSTM models. *J Mt Sci* 20: 1220-1231. <https://doi.org/10.1007/s11629-022-7606-0>
- Li ZL, Tang BH, Wu H, et al. (2013) Satellite-derived land surface temperature: Current status and perspectives. *Remote Sens Environ* 131: 14-37. <https://doi.org/10.1016/j.rse.2012.12.008>
- Loarie SR, Duffy PB, Hamilton H, et al. (2009) The velocity of climate change. *Nature* 462: 1052-1055. <https://doi.org/10.1038/nature08649>
- López-Tarazón JA, Bronstert A, Thielen AH, et al. (2019) The effects of global change on floods, fluvial geomorphology and related hazards in mountainous rivers. *Sci Total Environ* 669: 7-10. <https://doi.org/10.1016/j.scitotenv.2019.03.026>
- Lu D, Mausel P, Brondizio E, et al. (2004) Change detection techniques. *Int J Remote Sens* 25: 2365-2401. <https://doi.org/10.1080/0143116031000139863>
- Mal S, Rani S, Maharana P (2022) Estimation of spatio-temporal variability in land surface temperature over the Ganga River Basin using MODIS data. *Geocarto Int* 37: 3817-3839. <https://doi.org/10.1080/10106049.2020.1869331>
- Maleki S, Khormali F, Karimi AR (2014) Introducing different flow direction algorithms to map topographic wetness index and soil organic carbon in a loess hillslope of Toshihan area, Golestan Province. Iran. *J Soil Water Conserv* 21(1): 145-162.
- Mansouri Daneshvar MR, Ebrahimi M, Nejadsoleymani H (2019) An overview of climate change in Iran: facts and statistics. *Environ Syst Res* 8: 1-10. <https://doi.org/10.1186/s40068-019-0135-3>
- Mansourmoghaddam M, Rousta I (2023) Investigating and modeling the effect of the composition and arrangement of the landscapes of Yazd city on the land surface temperature using machine learning and Landsat-8 and Sentinel-2 data. *IJRSGIS* 15(3): 1-26. <https://doi.org/10.48308/gijs.2023.102195>
- Mansourmoghaddam M, Rousta I, Zamani M, et al. (2023) Investigating and predicting land surface temperature (LST) based on remotely sensed data during 1987-2030 (A case study of Reykjavik city, Iceland). *Urban Ecosyst* 26: 337-359. <https://doi.org/10.1007/s11252-023-01337-9>
- Marzeion B, Kaser G, Maussion F, et al. (2018) Limited influence of climate change mitigation on short-term glacier mass loss. *Nat Clim Chang* 8: 305-308. <https://doi.org/10.1038/s41558-018-0093-1>
- Minder JR, Letcher TW, Liu C (2018) The character and causes of elevation-dependent warming in high-resolution simulations of Rocky Mountain climate change. *J Clim* 31: 2093-2113. <https://doi.org/10.1175/JCLI-D-17-0321.1>
- Minder JR, Mote PW, Lundquist JD (2010) Surface temperature lapse rates over complex terrain: Lessons from the Cascade Mountains. *J Geophys Res Atmos* 115: 1-13. <https://doi.org/10.1029/2009JD013493>
- Mirzayi M, Riyahi Bakhtiyari A, Salman Mahini A, et al. (2013) Investigating the land cover changes in Mazandaran Province using landscape ecology's metrics between 1984-2010. *Iran J Appl Ecol* 2(4): 37-55.
- Mokhtarian Pourzavareh M, Khodayari A, Kohandel M (2022) Sustainable development mountain tourism in Iran. *Sport Bus J* 2(2): 301-320. <https://doi.org/10.22051/sbj.2023.42023.1057>
- Monforte P, Ragusa MA (2022) Temperature trend analysis and investigation on a case of variability climate. *Mathematics* 10: 1-13. <https://doi.org/10.3390/math10132202>
- Musselman KN, Clark MP, Liu C, et al. (2017) Slower snowmelt in a warmer world. *Nat Clim Change* 7(3): 214-219. <https://doi.org/10.1038/nclimate3225>
- Nabizada AF, Rousta I, Dalvi M, et al. (2022) Spatial and temporal assessment of remotely sensed land surface temperature variability in Afghanistan during 2000-2021. *Climate* 10: 111. <https://doi.org/10.3390/cli10070111>
- Nabizada AF, Rousta I, Mozaffari G, et al. (2023) A remotely sensed study of the impact of meteorological parameters on vegetation for the eastern basins of Afghanistan. *Earth Sci Informatics* 16: 1293-1312. <https://doi.org/10.1007/s12145-023-00965-1>
- Naghizadeh H, Rasouly A, Sari Sarraf B, et al. (2019) The variability of the snow depth in the northern zone of Iran is based on the ECMWF Database of the ERA Interim Edition. *GEOEH* 8(2): 211-229.
- Naseri E, Massah Bavani A, Sadi T (2021) Detection and attribution of changing in seasonal variability cause of climate change (Case study: Hillsides of Central Southern Alborz Mountains). *JSAEH* 8(1): 93-110. <http://jsaeh.khu.ac.ir/article-1-3108-en.html>
- Nasiri V, Belouiu M, Asghar Darvishsefat A, et al. (2023) Mapping tree species composition in a Caspian temperate mixed forest based on spectral-temporal metrics and machine learning. *Int J Appl Earth Obs Geoinf* 116: 103154. <https://doi.org/10.1016/j.jag.2022.103154>
- Nigrelli G, Chiarle M (2023) 1991-2020 climate normal in the European Alps: focus on high-elevation environments. *J Mt Sci* 20: 2149-2163. <https://doi.org/10.1007/s11629-023-7951-7>
- Noroozi J, Körner C (2018) A bioclimatic characterization of high elevation habitats in the Alborz mountains of Iran. *Alp Bot* 128: 1-11. <https://doi.org/10.1007/s00035-018-0202-9>
- O'Neal M, Roth L, Hanson B, et al. (2010) A field-based model of the effects of landcover changes on daytime summer temperatures in the North Cascades. *Phys Geogr* 31: 137-155. <https://doi.org/10.2747/0272-3646.31.2.137>
- Olafsson H, Rousta I (2021) Influence of atmospheric patterns and North Atlantic Oscillation (NAO) on vegetation dynamics in Iceland using Remote Sensing. *Eur J Remote Sens* 54: 351-363. <https://doi.org/10.1080/22797254.2021.1931462>
- Parmesan C (2006) Ecological and evolutionary responses to recent climate change. *Annu Rev Ecol Evol Syst* 37: 637-669. <https://doi.org/10.1146/annurev.ecolsys.37.091305.110100>
- Petropoulos G, Kontoes C, Keramitsoglou I (2011) Burnt area delineation from a uni-temporal perspective based on Landsat TM

- imagery classification using Support Vector Machines. *Int J Appl Earth Obs Geoinf* 13(1): 70–80.
<https://doi.org/10.1016/j.jag.2010.06.008>
- Pepin NC, Seidel DJ (2005) A global comparison of surface and free-air temperatures at high elevations. *J Geophys Res D Atmos* 110: 1-15. <https://doi.org/10.1029/2004JD005047>
- Pepin N, Bradley RS, Diaz HF, et al. (2015) Elevation-dependent warming in mountain regions of the world. *Nat Clim Chang* 5: 424-430. <https://doi.org/10.1038/nclimate2563>
- Pflugmacher D, Rabe A, Peters M, et al. (2019) Mapping pan-European land cover using Landsat spectral-temporal metrics and the European LUCAS survey. *Remote Sens Environ* 221: 583-595. <https://doi.org/10.1016/j.rse.2018.12.001>
- Qie Y, Wang N, Wu Y, et al. (2020) Variations in winter surface temperature of the Purog Kangri Ice Field, Qinghai-Tibetan Plateau, 2001-2018, using MODIS data. *Remote Sens* 12: 1133. <https://doi.org/10.3390/rs12071133>
- Rangwala I, Miller JR (2012) Climate change in mountains: A review of elevation-dependent warming and its possible causes. *Clim Change* 114: 527-547. <https://doi.org/10.1007/s10584-012-0419-3>
- Rangwala I, Sinsky E, Miller JR (2013) Amplified warming projections for high altitude regions of the northern hemisphere mid-latitudes from CMIP5 models. *Environ Res Lett* 8: 024040. <https://doi.org/10.1088/1748-9326/8/2/024040>
- Rani S, Mal S (2022) Trends in land surface temperature and its drivers over the High Mountain Asia. *Egypt J Remote Sens Sp Sci* 25: 717-729. <https://doi.org/10.1016/j.ejrs.2022.04.005>
- Roshan G, Faghani M, Fitchett JM (2020) Developing a thermal stress map of Iran through modeling a combination of bioclimatic indices. *Environ Monit Assess* 192: 1-21. <https://doi.org/10.1007/s10661-020-08503-y>
- Roshan G, Yousefi R, Fitchett JM (2016) Long-term trends in tourism climate index scores for 40 stations across Iran: the role of climate change and influence on tourism sustainability. *Int J Biometeorol* 60: 33-52. <https://doi.org/10.1007/s00484-015-1003-0>
- Rousta I, Doostkamian M, Taherian AM, et al. (2017) Investigation of the spatio-temporal variations in atmosphere thickness pattern of Iran and the middle east with special focus on precipitation in Iran. *Climate* 5: 82. <https://doi.org/10.3390/cli5040082>
- Rousta I, Olafsson H, Nasserzadeh MH, et al. (2021) Dynamics of daytime land surface temperature (Lst) variabilities in the middle east countries during 2001-2018. *Pure Appl Geophys* 178: 2357-2377. <https://doi.org/10.1007/s00024-021-02765-4>
- Rousta I, Olafsson H, Zhang H, et al. (2022) Anthropogenic factors affecting the vegetation dynamics in the arid Middle East. *Environ Clim Technol* 26: 774-805. <https://doi.org/10.2478/rtuct-2022-0060>
- Sabziparvar AA, Mir Mousavi SH, Karampour M, et al. (2019) Harmonic analysis of the spatiotemporal pattern of thunderstorms in Iran (1961-2010). *Adv Meteorol* 2019:1-14. <https://doi.org/10.1155/2019/1612503>
- Sambuco EN, Mark BG, Patrick N, et al. (2020) Mountain Temperature changes from embedded sensors spanning 2000 m in Great Basin National Park, 2006-2018. *Front Earth Sci* 8:1-18. <https://doi.org/10.3389/feart.2020.00292>
- Sarhan E, Mofidi A, Dadashi-Roudbari A, et al. (2023) Climatology of cold spots and LST minimums in Iran using high-resolution satellite data. *Theor Appl Climatol*. <https://doi.org/10.1007/s00704-023-04699-4>
- Scherrer SC, Ceppi P, Croci-Maspoli M, et al. (2012) Snow-albedo feedback and Swiss spring temperature trends. *Theor Appl Climatol* 110: 509-516. <https://doi.org/10.1007/s00704-012-0712-0>
- Seleshi Y, Zanke U (2004) Recent changes in rainfall and rainy days in Ethiopia. *Int J Climatol* 24: 973-983. <https://doi.org/10.1002/joc.1052>
- Shahnaz R, Golamhasan M, Saeed J, et al. (2023) On the nature of Caspian clouds. *J Meteorol Res* 37: 262-272. <https://doi.org/10.1007/s13351-023-2167-x>
- Sörensen R, Zinko U, Seibert J (2006) On the calculation of the topographic wetness index: evaluation of different methods based on field observations. *Hydrol Earth Syst Sci* 10(1): 101-112. <https://doi.org/10.5194/hess-10-101-2006>
- Steiger R, Knowles N, Pöll K, et al. (2022) Impacts of climate change on mountain tourism: a review. *J Sustain Tour* 0: 1-34. <https://doi.org/10.1080/09669582.2022.2112204>
- Taherizadeh M, Khushemehr JH, Niknam A, et al. (2023) Revealing the effect of an industrial flash flood on vegetation area: a case study of Khusheh Mehr in Maragheh-Bonab Plain, Iran. *Remote Sens Appl: Soc Environ* 32: 101016. <https://doi.org/10.1016/j.rsase.2023.101016>
- Tan J, Noureddeen N, Mao K, et al. (2019) Deep learning convolutional neural network for the retrieval of land surface temperature from AMSR2 data in China. *Sensors (Switzerland)* 19: 2987. <https://doi.org/10.3390/s19132987>
- Tang Z, Deng G, Hu G, et al. (2022) Satellite observed spatiotemporal variability of snow cover and snow phenology over high mountain Asia from 2002 to 2021. *J Hydrol* 613: 128438. <https://doi.org/10.1016/j.jhydrol.2022.128438>
- Tayanç M, İm U, Doğruel M, et al. (2009) Climate change in Turkey for the last half century. *Clim Change* 94: 483-502. <https://doi.org/10.1007/s10584-008-9511-0>
- Vaghefi SA, Keykhai M, Jahanbakhshi F, et al. (2019) The future of extreme climate in Iran. *Sci Rep* 9: 1-11. <https://doi.org/10.1038/s41598-018-38071-8>
- Vakili Tajareh F, Bayat A, Rahmani M, et al. (2022) Zonation of flood susceptibility and determining the factors affecting it using the Maximum Entropy Method. *IJWMSE* 16(59): 1-11. <http://jwmsei.ir/article-1-1029-en.html>
- Viviroli D, Archer DR, Buytaert W, et al. (2011) Climate change and mountain water resources: Overview and recommendations for research, management and policy. *Hydrol Earth Syst Sci* 15: 471-504. <https://doi.org/10.5194/hess-15-471-2011>
- Viviroli D, Kumm M, Meybeck M, et al. (2020) Increasing dependence of lowland populations on mountain water resources. *Nat Sustain* 3: 917-928. <https://doi.org/10.1038/s41893-020-0559-9>
- Vuille M, Bradley RS (2000) Mean annual temperature trends and their vertical structure in the tropical Andes. *Geophys Res Lett* 27(23): 3885-3888. <https://doi.org/10.1029/2000GL011871>
- Wang QX, Wang MB, Fan XH (2018) Seasonal patterns of warming amplification of high-elevation stations across the globe. *Int J Climatol* 38: 3466-3473. <https://doi.org/10.1002/joc.5509>
- Wang X, Chen R, Li H, et al. (2022) Detection and attribution of trends in flood frequency under climate change in the Qilian Mountains, Northwest China. *J Hydrol Reg Stud* 42: 101153. <https://doi.org/10.1016/j.ejrh.2022.101153>
- Willibald F, Kotlarski S, Ebner PP, et al. (2021) Vulnerability of ski tourism towards internal climate variability and climate change in the Swiss Alps. *Sci Total Environ* 784: 147054. <https://doi.org/10.1016/j.scitotenv.2021.147054>
- Xiao X, Perry EE, Gao J, et al. (2020) Winter tourism and climate change: Exploring local and non-local snowmobilers' perceptions of climate change and adaptation behaviors. *J Outdoor Recreat Tour* 31:100299. <https://doi.org/10.1016/j.jort.2020.100299>
- Yan L, Liu Z, Chen G, et al. (2016) Mechanisms of elevation-dependent warming over the Tibetan plateau in quadrupled CO2 experiments. *Clim Change* 135: 509-519. <https://doi.org/10.1007/s10584-016-1599-z>
- Yang T, Li Q, Hamdi R, et al. (2022) Trends and spatial variations of rain-on-snow events over the high Mountain Asia. *J Hydrol* 614: 128593. <https://doi.org/10.1016/j.jhydrol.2022.128593>
- Yang YZ, Cai WH, Yang J (2017) Evaluation of MODIS land surface temperature data to estimate near-surface air temperature in Northeast China. *Remote Sens* 9:1-19. <https://doi.org/10.3390/rs9050410>
- Yousefizadeh R, Sehatkashani S, Gholamnia K, et al. (2022) Investigating the trend of changes and snow prediction in Alborz heights of Mazandaran province in winter, using satellite image processing. *Clim Res* 1400(48): 157-175.
- Zemp M, Huss M, Thibert E, et al. (2019) Global glacier mass changes and their contributions to sea-level rise from 1961 to 2016. *Nature* 568: 382-386. <https://doi.org/10.1038/s41586-019-1071-0>
- Zhang H, Zhang F, Zhang G, et al. (2016) Evaluation of cloud effects on air temperature estimation using MODIS LST based on ground measurements over the Tibetan Plateau. *Atmos Chem Phys* 16: 13681-13696. <https://doi.org/10.5194/acp-16-13681-2016>